Research Square

Preprints are preliminary reports that have not undergone peer review.
They should not be considered conclusive, used to inform clinical practice,
or referenced by the media as validated information.

# Mechanical compression reprograms cell states associated with patient survival and therapy response

**Styliana Georgiou**
University of Cyprus
**Chrystalla Stylianou**
University of Cyprus
**Ekaterini Himonas**
Cyprus Institute of Neurology and Genetics
**Sotiris Kyriakou**
Cyprus Institute of Neurology and Genetics
**Fotios Mpekris**
Cyprus Institute of Neurology and Genetics
**Chrysovalantis Voutouri**
AnaBioSi-Data Ltd
**Triantafyllos Stylianopoulos**
University of Cyprus
**Maria Kalli**
mkalli02@ucy.ac.cy

University of Cyprus

**Research Article**

**Keywords:** compressive force, solid stress, drug resistance, pancreatic cancer, liver cancer, breast cancer, transcriptomics, metabolomics, precision oncology

**Posted Date:** April 1st, 2026

**DOI:** https://doi.org/10.21203/rs.3.rs-9276682/v1

**License:** This work is licensed under a Creative Commons Attribution 4.0 International License.
Read Full License

**Additional Declarations:** The authors declare no competing interests.

# Mechanical compression reprograms cell states associated with patient survival and therapy response

Styliana Georgiou[1,2], Chrystalla Stylianou[1], Ekaterini Himonas[3], Sotiris Kyriakou[3], Fotios Mpekris[3], Chrysovalantis Voutouri[1,2], Triantafyllos Stylianopoulos[1,*] and Maria Kalli[1,*]

[1]Cancer Biophysics Laboratory, Department of Mechanical and Manufacturing Engineering, University of Cyprus, Nicosia, Cyprus

[2] AnaBioSi-Data Ltd, Nicosia, Cyprus

[3]Cancer Genetics, Therapeutics & Ultrastructural Pathology Department, The Cyprus Institute of Neurology & Genetics, Nicosia, Cyprus

*Correspondence to mkalli02@ucy.ac.cy ; tstylian@ucy.ac.cy

**Abstract**

Precision oncology frameworks primarily rely on tumor-intrinsic molecular features to guide therapeutic decision-making, yet the contribution of mechanical forces within the tumor microenvironment remains poorly defined. Here, we investigate how compressive stress, a fundamental mechanical force arising during tumor growth, reshapes tumor cell states and modulates clinically relevant therapeutic pathways. Using a controlled compression system, we comprehensively profiled transcriptional responses in pancreatic cancer cells and integrated these with datasets from mechanically compressed breast and liver cancer models. Compression induced extensive, tumor type–specific transcriptional reprogramming, characterized by activation of stress-adaptive pathways and suppression of proliferative programs. Gene-level overlap was limited between tumor types, though partial convergence emerged at the pathway level. Compression-associated transcriptional signatures were independent of pre-existing genomic alterations, yet detectable in patient tumors across TCGA cohorts, underscoring their clinical relevance. Higher compression signature scores were associated with reduced survival in pancreatic and liver cancers, but not breast cancer, revealing tumor type–specific prognostic associations. Integration with pharmacogenomic databases showed that compression-responsive genes intersect with multiple drug-target networks in pancreatic cancer, including inflammatory, angiogenic, and kinase signaling pathways. Complementary metabolomic profiling identified coordinated alterations in purine metabolism, sphingolipid signaling, and redox pathways, further linking mechanical stress to drug-relevant cellular processes. Together, these findings identify tumor compression as a regulator of molecular states that interface with therapeutic targets and patient outcomes. Incorporating compression-associated molecular signatures into precision oncology frameworks may improve the identification of therapeutic vulnerabilities and prediction of treatment response in solid tumors.

**Conflicts of interest**

The authors declare no potential conflicts of interest.

**Running title**

Tumor compression reshapes therapy-relevant molecular states

## Significance statement

Tumor compression reprograms cancer cell states independently of genomic alterations, generating context-specific molecular states detectable in-patient tumors that associate with survival and intersect with therapeutic targets in pancreatic cancer.

## Introduction

Genetic and epigenetic alterations drive tumor initiation and progression by activating oncogenic signaling pathways, disabling tumor suppressor programs, and reshaping cellular behavior (1). Cancer treatment strategies, including cytotoxic chemotherapy, targeted therapies, and immunotherapies, have therefore been developed to eliminate rapidly proliferating cells or exploit tumor-specific molecular dependencies. In addition, combination regimens aim to suppress compensatory signaling networks that arise during treatment. However, despite the availability of numerous therapies, achieving durable survival benefits remains challenging, as many tumors develop adaptive resistance (2, 3). This resistance reflects not only continued genetic evolution but also dynamic transcriptional reprogramming and phenotypic plasticity that enable cancer cells to withstand therapy (4).

To address this complexity, precision oncology frameworks incorporate molecular biomarkers into therapeutic decision-making. Large-scale multi-omics initiatives, including The Cancer Genome Atlas (TCGA), the International Cancer Genome Consortium (ICGC), and the Clinical Proteomic Tumor Analysis Consortium (CPTAC), have systematically defined tumor genomic alterations, transcriptional profiles, proteomic changes, and metabolic states (5-7). These efforts have improved molecular stratification and informed biomarker-driven therapy selection (8, 9). However, clinical responses remain limited across many solid malignancies, indicating that tumor-intrinsic molecular features alone do not fully explain therapeutic outcomes.

In addition to tumor-intrinsic molecular alterations, the tumor microenvironment (TME) contributes to disease progression and therapeutic response (10, 11). As solid tumors grow, the surrounding tissue undergoes substantial structural remodeling. Cellular proliferation and extracellular matrix (ECM) deposition and stiffening, progressively alter tissue architecture and generate mechanical forces that reshape the physical environment in which cancer cells reside (12). At the tissue level, these biomechanical changes affect vascular integrity, interstitial fluid transport, and immune cell infiltration, thereby influencing drug delivery and treatment efficacy (13-15). Beyond these structural effects, mechanical stress also acts directly on the cellular components of the TME, modulating signaling pathways and cellular states that influence therapeutic response (16).

Elevated ECM stiffness is the most extensively characterized mechanical parameter within this context. Increased ECM rigidity, determined by matrix composition and organization, has been associated with malignant progression through integrin clustering, focal adhesion kinase (FAK) activation, cytoskeletal tension, and YAP/TAZ-dependent transcriptional regulation (17). Experimental systems employing tunable hydrogels and engineered matrices have demonstrated that stiffness modulates proliferation, survival signaling, metabolic adaptation, and invasive behavior, as well as drug efficacy (18-21).

However, stiffness does not directly represent the mechanical forces acting within a growing tumor. While stiffness reflects resistance to deformation, tumor expansion within confined tissues generates compressive loads that may not scale proportionally with matrix rigidity (20, 22, 23). Substantial compressive forces can arise even in tumors with slight increases in

stiffness, and conversely, increased rigidity does not necessarily imply higher intratumoral mechanical stress (22). Distinguishing between material stiffness and compressive forces is therefore critical for a comprehensive understanding of how the physical microenvironment regulates tumor progression and treatment response.

Prior work from our group has demonstrated that compressive forces regulate cancer cell behavior through distinct, tumor type–specific mechanisms. In pancreatic cancer, mechanical compression activates the PI3K/Akt pathway and drives cytoskeletal remodeling via p38 MAPK, JNK, and small GTPase signaling, collectively enhancing migratory capacity (24, 25). Beyond these cell-intrinsic effects, compression also activates fibroblasts, which in turn promote pancreatic cancer cell migration through the secretion of signaling molecules such as GDF15 (26). In contrast, in brain cancer cells, compression-induced migration is mediated through a distinct mechanism involving activation of the MEK1/ERK1 pathway (27). Compressive stress has further been shown to induce autophagy as a stress-adaptive survival response, contributing to reduced sensitivity to cytotoxic therapies (28).

Together, these findings underscore that mechanical compression reprograms signaling pathways with direct implications for tumor aggressiveness and treatment resistance. However, these insights have largely emerged from focused, hypothesis-driven studies interrogating individual pathways in isolation. At the same time, therapeutic strategies continue to expand, with an increasing number of targeted and combination treatments being developed to exploit tumor-specific vulnerabilities. Yet, how mechanical forces within the TME influence the molecular context in which these drugs operate remains poorly understood. This gap is critical, as mechanical stress may alter cellular states in ways that unpredictably modulate drug mechanisms of action and efficacy. A comprehensive, multi-layered analysis integrating transcriptional, metabolic, and functional responses to compression, and their intersection with oncogenic dependencies and pharmacological vulnerabilities, remains lacking.

To address this gap, we exposed pancreatic cancer cells to defined compressive stress and performed systematic transcriptomic profiling to map compression-induced gene expression programs. Integration of publicly available transcriptomic datasets from mechanically compressed breast and liver cancer cells enabled the identification of conserved and context-specific compression signatures across tumor types. These signatures were mapped against oncogenic alteration landscapes and patient-derived tumor transcriptomes, and interrogated against pharmacogenomic databases to identify intersections with actionable therapeutic targets. Complementary Liquid Chromatography–Mass Spectrometry (LC-MS)–based (exo)metabolomic profiling was performed to determine whether compressive forces engage metabolic reprogramming that converges on therapeutically relevant pathways. Together, this work positions tumor compression as a biologically and clinically relevant variable within a mechanically informed precision oncology framework, and provides a foundation for understanding how mechanical forces interact with genetic and metabolic programs to shape therapeutic response.

## Methods

*Cell culture*

Human pancreatic MIA PaCa-2 cancer cells were obtained from the American Type Culture Collection (ATCC, CRL-1420) and maintained in Dulbecco's Modified Eagle Medium (DMEM) supplemented with 10% fetal bovine serum (FBS) and 1% antibiotic-antimycotic solution. Cells were cultured at 37 °C in a humidified incubator with 5% $CO_2$ and routinely passaged at approximately 70–80% confluence using standard trypsinisation procedures. Cells were regularly tested and confirmed to be free of mycoplasma contamination.

*Application of mechanical compression*

For the application of defined and controlled compression on MIA PaCa-2 cells, our previously described transmembrane pressure device was employed (26). In brief, 24 hours prior to compression, cells were seeded at a density of $2.0 \times 10^5$ cells in the upper chamber of a 24 mm diameter Transwell insert with 0.4 µm pores (Greiner Bio-One). The cell monolayer was covered with a 2% low-melting agarose cushion, and a piston with adjustable weight was placed on top to generate 4 mmHg of pressure for 24 hours. This level of compression was selected based on our previous studies demonstrating that it elicits robust and reproducible functional responses in cancer cells, including alterations in signaling and migratory behavior (26). Control cells were covered with agarose cushion only.

*RNA-seq and differential expression analysis*

For pancreatic cancer, RNA-seq data were generated in this study using MIA PaCa-2 cells exposed to mechanical compression (4 mmHg) or maintained under control (uncompressed) conditions, with three biological replicates per condition. Following compression, cells were immediately washed with ice-cold PBS and harvested for RNA extraction. Total RNA was isolated using the RNeasy Plus Mini Kit (Qiagen) according to the manufacturer's instructions. Library preparation was performed using the TruSeq Stranded mRNA LT Sample Prep Kit (Illumina), and paired-end sequencing (101 bp reads) was carried out on an Illumina platform by Macrogen Inc. (Seoul, South Korea). Read quality was assessed using FastQC (v0.11.7), and adapter and quality trimming were performed with Trimmomatic (v0.38). Trimmed reads were aligned to the *Homo sapiens* reference genome (GRCh38) using the splice-aware aligner HISAT2 (v2.2.1), and transcript abundances were quantified with StringTie (v2.1.3b) to obtain gene-level count matrices.

For breast and liver cancer, bulk RNA-seq datasets were obtained from the Gene Expression Omnibus (GEO). Breast cancer data were derived from MDA-MB-231 cells subjected to solid stress compression (GSE282791; 1546 Pa vs. 0 Pa, n = 6 per group, 16 h compression). These samples were sequenced by Novogene, aligned to GRCh38 using STAR (v2.7.9a), and originally processed with edgeR using TMM normalisation and limma-voom for differential expression. For inclusion in the present cross-tissue analysis, raw count matrices were reprocessed through our uniform DESeq2 pipeline (see below). Liver cancer data were obtained from HepG2 and Hep3B cells exposed to mechanical compression for 5 days (GSE231717; compressed vs. control, n = 2 per cell line per group), originally aligned with STAR to GRCh38 and analysed with DESeq2.

For uniform cross-tissue comparison, all datasets were processed through DESeq2 (v1.50.2) with the median-of-ratios normalisation method. A pre-filtering threshold of ≥10 counts in ≥3 samples was applied. For multi-cell-line datasets (liver), cell line was included as a covariate

in the design formula. Analyses were performed independently for each cancer type to avoid confounding effects arising from cell line–specific transcriptional programmes. $Log_2$ fold change estimates were refined using apeglm shrinkage, and differentially expressed genes (DEGs) were defined as Benjamini–Hochberg adjusted $P < 0.05$ and $|log_2FC| \geq 1$. Gene identifiers were mapped to HGNC symbols using org.Hs.eg.db.

*Gene set enrichment analysis*

GSEA was performed using clusterProfiler on gene lists ranked by unshrunken $log_2FC$ and converted to Entrez IDs. Three databases were queried per cancer type: KEGG (gseKEGG; minimum/maximum gene set size 10/500), GO Biological Process (gseGO; 15/500), and Reactome (gsePathway via ReactomePA; 15/500). All analyses used Benjamini–Hochberg correction with adjusted $P < 0.05$. Shared pathways across tumour types were identified by matching enriched Reactome pathway names across all three cancer types and visualised using UpSet plots. Gene–pathway networks for shared Reactome pathways were constructed using igraph.

*Validation against pre-existing genomic alterations*

To confirm that compression-responsive DEGs reflect mechanical stimuli rather than pre-existing genomic backgrounds, DEGs were cross-referenced against three layers of DepMap data (release 25Q3) for each cell line: somatic mutations (Fisher's exact test for enrichment), copy number alterations (gene-level relative copy number thresholds: <0.5 deep deletion, >3.0 amplification, relative to a diploid baseline of 1.0), and baseline expression outliers (|z-score| > 2 across all DepMap cell lines). Each DEG was classified as compression-driven (no alteration), single-layer alteration, or multi-layer alteration. Pathway-level breakdowns were generated for top Reactome GSEA pathways.

*Clinical validation in TCGA and GTEx cohorts*

Expression data from TCGA (BRCA, LIHC, PAAD) and GTEx normal tissues were obtained via the UCSC Xena platform (TcgaTargetGtex cohort), which provides uniformly STAR-aligned, RSEM-quantified $log_2(TPM + 0.001)$ values across all samples. Cancer-matched compression signatures were defined by splitting significant DEGs into upregulated and downregulated gene sets. Compression scores were computed using ssGSEA (GSVA package), selected as the primary metric after confirming high inter-method concordance (Spearman $\rho > 0.8$) across three alternative scoring approaches (mean expression ratio, z-score, and $log_2FC$-weighted z-score). Clinical associations were evaluated by comparing compression scores between tumour, TCGA adjacent normal, and GTEx normal samples (Wilcoxon rank-sum tests), stage progression analysis (Jonckheere–Terpstra trend test), and survival analysis (Kaplan–Meier with log-rank test; univariate and multivariate Cox regression adjusting for stage, age, and sex) for overall survival and progression-free interval.

*Drug–gene interaction analysis*

To map compression-responsive genes to the pancreatic cancer therapeutic landscape, all drugs with clinical trial evidence in pancreatic cancer were compiled from the Open Targets Platform using verified disease identifiers (EFO_0002618, MONDO_0005184, EFO_1000044, EFO_0003860, EFO_1000359) with complete pagination to avoid row-limit truncation. Each drug was classified into a single mechanistic category based on its primary mechanism of action annotation in Open Targets. Trial phases reflect the highest phase recorded across

pancreatic cancer indications. Non-therapeutic agents (e.g., bupivacaine, propofol, dexamethasone) were excluded.

Drug–gene interactions for compression DEGs were queried via the DGIdb 5.0 GraphQL API in batches of 50 genes, retrieving interaction scores, publication counts, and source databases. Interactions were cross-referenced with the Open Targets PDAC drug list to identify compression DEGs targeted by clinically investigated agents. Drug–gene pairs with interaction scores ≥0.1 were retained for the gene × drug interaction map; this threshold was chosen to balance sensitivity (retaining standard-of-care chemotherapy agents, which receive lower per-gene scores due to their broad mechanism of action) with specificity (excluding poorly supported associations). Results were additionally cross-validated against CIViC clinical evidence (nightly TSV release; predictive evidence levels A–D) with disease-specific keyword matching.

*Exometabolomic profiling and analysis*

To assess extracellular metabolic changes induced by mechanical compression, LC-MS-based exometabolomic profiling was performed on conditioned media collected from MIA PaCa-2 cells exposed to 4 mmHg compression, as described above. LC-MS analysis was normalised to the number of cells seeded per condition. Conditioned media samples (750 µL) were collected after 24 hours of compression. Media were clarified by centrifugation to remove cellular debris and stored at −80 °C until analysis. Control samples included fresh DMEM without cells processed in parallel. Three independent biological replicates were analysed per condition.

Methanol and acetonitrile were purchased from Honeywell, and formic acid from ThermoFisher. Ammonium acetate and ammonium formate were purchased from Fluorochem (Derbyshire, UK), whereas purine and hexakis(1H, 1H, 3H-tetrafluoropropoxy) phosphazine (HP-0921) were supplied by Agilent Technologies (Santa Clara, CA, USA). All solvents were LC-MS grade; all reagents were of >99% purity and used without further purification.

For exometabolite extraction, 50 µL of thawed culturing media was mixed with 500 µL of ice-cold extraction mixture (50% methanol, 30% acetonitrile, 20% $H_2O$), vortexed for 30 s, incubated at 4 °C for 5 min, and centrifuged at 16,000 × *g* for 15 min at −20 °C. Supernatants were transferred to LC-MS vials and stored at −80 °C until analysis.

Mass spectrometric analysis was carried out on an Agilent REVIDENT Q-TOF mass spectrometer coupled to an Agilent 1290 Infinity II UPLC system via Dual AJS ESI (Agilent Technologies, Santa Clara, CA, USA). Chromatographic separation used an Agilent InfinityLab Poroshell 120 HILIC-Z column (2.1 × 150 mm, 2.7 µm) with ammonium formate/acetonitrile (positive mode) and ammonium acetate/acetonitrile (negative mode) mobile phases. Full chromatographic gradients and mass spectrometric parameters are provided in Supplementary Methods.

Tentative metabolite identifications were made using the Agilent MassHunter METLIN Metabolomics Database (PCDL Manager v B.08.00), with precursor ion m/z tolerances of ±10 ppm plus 2 mDa and a library match score threshold of 70. Raw peak tables were filtered to retain only annotated metabolites with valid HMDB or LIPID MAPS identifiers.

All downstream statistical analysis was performed using MetaboAnalyst 6.0 (www.metaboanalyst.ca). All nine samples (three compressed, three control, and three cell-free 0-hour media controls) were jointly processed with $\log_{10}$ transformation and Pareto scaling. Media-only samples were subsequently removed prior to differential analysis, which was carried out between 0 mmHg and 4 mmHg conditions using Welch's t-test. Metabolites meeting a significance threshold of $p < 0.05$ and $|\log_2 FC| \geq 1.0$ were retained as significantly altered. For visualisation, significant metabolites from both ionisation modes were combined into a single heatmap with Z-score normalisation per metabolite, Euclidean distance, and Ward's D2 clustering. Pathway enrichment analysis was performed using over-representation analysis (ORA) against the RaMP pathway library with hypergeometric testing; pathways with $p < 0.05$ were considered significant. Enriched pathway names were further consolidated into higher-order functional categories for cross-condition comparison.

*Software and statistical analysis*

RNA-seq and pathway analyses were performed in R (v4.5.0) using DESeq2 (v1.50.2), clusterProfiler, ReactomePA, and GSVA. Drug–gene interaction queries were implemented in Python 3.11. Visualisations used ggplot2, pheatmap, EnhancedVolcano, igraph/ggraph (R), and matplotlib/seaborn (Python). TCGA data were accessed via UCSCXenaTools. All tests were two-sided; Benjamini–Hochberg correction was applied unless otherwise stated, with adjusted $P < 0.05$ considered significant.

*Data Availability*

The RNA-seq data generated in this study are available from the corresponding author upon reasonable request. Publicly available datasets used in this study include GSE282791 (breast) and GSE231717 (liver), obtained from the Gene Expression Omnibus. TCGA and GTEx expression data were accessed via the UCSC Xena platform (TcgaTargetGtex cohort). DepMap genomic alteration data are available at depmap.org (release 25Q3).

## Results

### Mechanical compression induces context-dependent transcriptional reprogramming across tumor types

To comprehensively define the transcriptional architecture underlying compression-induced adaptation, we subjected human pancreatic cancer cells (Mia PaCa-2) to a controlled compressive force (4 mmHg) using our established transmembrane pressure system and performed genome-wide transcriptomic profiling. We further evaluated the cross-tumor conservation of these mechano-adaptive programs through integrative analysis of publicly available transcriptomic datasets from mechanically compressed breast (MDA-MB-231) and hepatocellular carcinoma (HepG2 and Hep3B) cell lines. Breast cancer cells were exposed to increasing levels of compression using the same platform, ranging up to 11.6 mmHg; for cross-tumor comparisons, we focused on the highest condition, which elicited the most robust transcriptional response (29). In contrast, liver cancer cells were subjected to volumetric compression induced by osmotic loading and spatial confinement, generating a sustained, highly compressed state without direct application of externally controlled pressure (30). Although the mode and magnitude of compression are not directly equivalent across systems, all approaches model mechanical confinement within tumors and induce comparable mechano-adaptive transcriptional responses.

Differential expression analysis revealed extensive transcriptional remodeling in pancreatic cancer cells subjected to mechanical compression (**Fig. 1A**). A substantial number of genes were significantly altered, with a predominance of upregulated transcripts. Hierarchical clustering demonstrated clear segregation between control and compressed samples (**Fig. 1B**), indicating a robust and coordinated response. Compression induced stress-associated genes including *GADD45A* and *NUPR1*, and the mechanosensitive regulators *SERPINE1* and *VEGFA,* alongside metabolic regulators such as *HK2, ENO2*, and *PFKFB4*, and inflammatory mediators including *IL6R* and *CXCL8*, consistent with activation of adaptive stress, inflammatory, and metabolic programs. To determine whether these gene-level alterations reflect specific biological pathways, we performed gene set enrichment analysis (GSEA) using Reactome annotations (**Fig. 2A**). Compression prominently activated integrated response and proteostasis networks, including PERK-regulated gene expression, ATF4-mediated transcription, EIF2AK4/GCN2 signaling, and unfolded protein response (UPR) pathways. These programs were accompanied by activation of cholesterol biosynthesis and nutrient-sensing pathways, including amino acid transport across the plasma membrane and SLC-mediated amino acid transport, suggesting coordinated metabolic adaptation to compression-induced nutrient limitation. NRF2-dependent redox signaling and PI3K/AKT-related pathways were also enriched, supporting cytoprotective and metabolic reprogramming. In contrast, mitotic cell cycle processes, including chromosome segregation, DNA replication, and cell cycle progression, were strongly suppressed

Mechanical compression similarly induced marked transcriptional changes in breast cancer cells (**Fig. 1A**), with heatmap analysis demonstrating distinct clustering between conditions (**Fig. 1C**). Upregulated genes included transcription factors and stress regulators such as *JUN, MYC, CEBPB, DUSP1*, and the stress-inducible transcription factor *ATF3*, as well as EMT-associated factors including *SNAI1*, suggest activation of transcriptional plasticity and migratory potential. Consistent with these gene-level patterns, GSEA revealed enrichment of pathways related to transcriptional regulation, rRNA processing, peptide elongation, and

amino acid deprivation signaling via *EIF2AK4/GCN2* (**Fig. 2B**). Notably, cellular response to starvation was significantly activated, mirroring the nutrient-stress axis observed in pancreatic cells. Concurrent suppression of DNA replication, homologous recombination, pre-replication complex activation, and mitotic progression pathways mirrored the proliferative repression observed in pancreatic cells. Thus, breast cancer cells exhibit a stress-responsive and translational control program under compression, coupled with coordinated downregulation of cell cycle machinery.

In hepatocellular carcinoma models, compression elicited significant differential gene expression (**Fig. 1A**), while a baseline heterogeneity between HepG2 and Hep3B cells was observed (**Fig. 1D**). Upregulated genes included *VEGFA, PDGFB, ANGPTL4, AXL*, the hypoxia- and stress-responsive factor *NDRG1*, and ECM regulators, suggest enhanced extracellular signaling and microenvironmental adaptation. GSEA further demonstrated strong activation of ECM organization, collagen formation, integrin cell surface interactions, proteoglycan remodeling, and growth factor–associated pathways (**Fig. 2C**). Platelet degranulation and hemostasis-related pathways were also enriched, highlighting structural and paracrine adaptation. In contrast to these activated programs, several DNA replication and genome maintenance pathways were suppressed, including ATR activation in response to replication-associated DNA damage, suggesting impaired ATR signaling under compression. As in pancreatic and breast models, S-phase progression and mitotic checkpoint pathways were significantly suppressed. These data indicate that liver cancer cells respond to compression predominantly through matrix remodeling and structural reorganization, while similarly reducing proliferative signaling.

Together, these results show that mechanical compression induces a shared adaptive response that is shaped by tumor type–specific transcriptional programs.

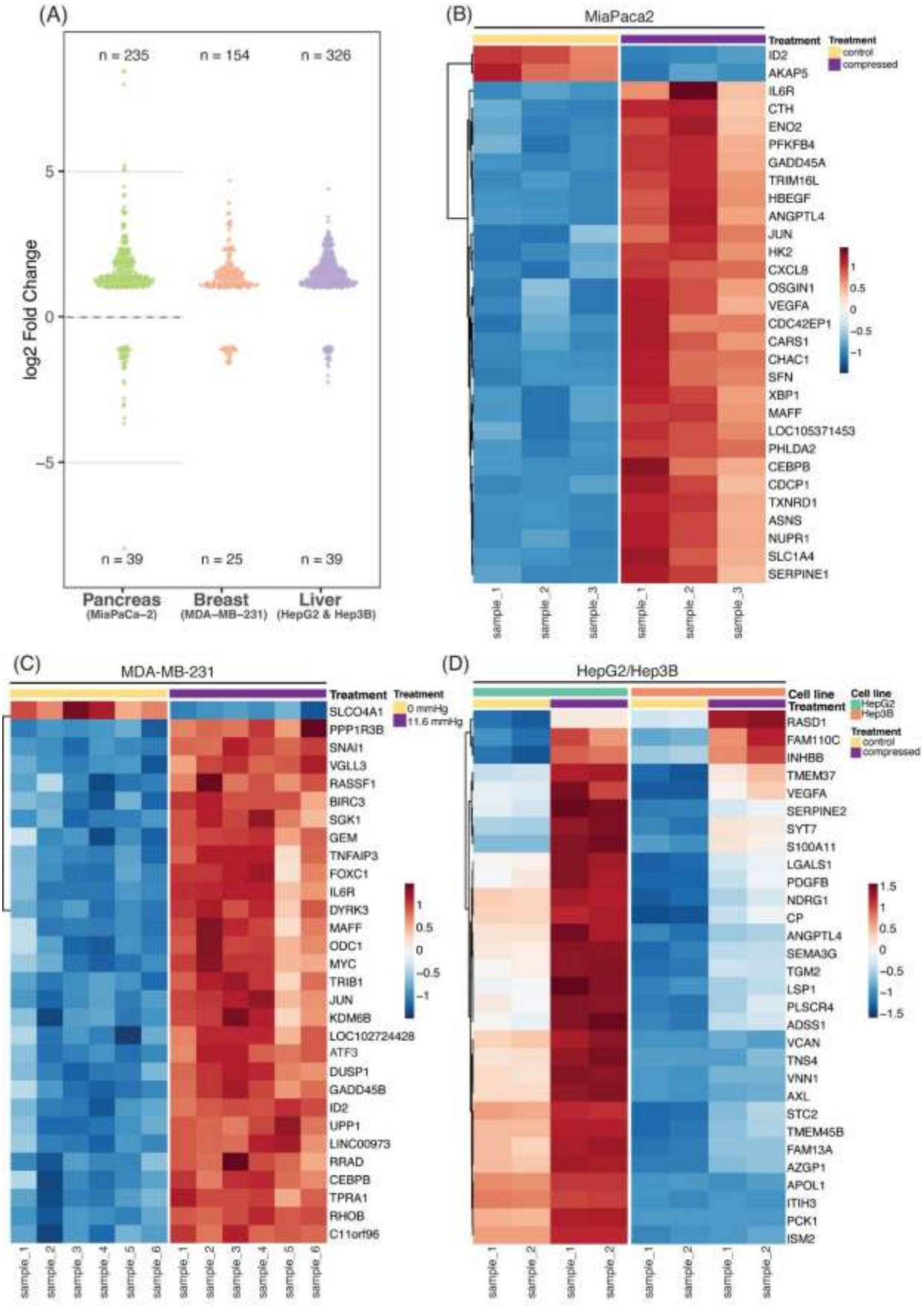

(A)
n = 235
n = 154
n = 326
log2 Fold Change
5
0
−5
n = 39
n = 25
n = 39
Pancreas
(MiaPaCa−2)
Breast
(MDA−MB−231)
Liver
(HepG2 & Hep3B)
(B)
MiaPaca2
Treatment
Treatment
control
compressed
ID2
AKAP5
IL6R
CTH
ENO2
PFKFB4
GADD45A
TRIM16L
HBEGF
ANGPTL4
JUN
HK2
CXCL8
OSGIN1
VEGFA
CDC42EP1
CARS1
CHAC1
SFN
XBP1
MAFF
LOC105371453
PHLDA2
CEBPB
CDCP1
TXNRD1
ASNS
NUPR1
SLC1A4
SERPINE1
1
0.5
0
−0.5
−1
sample_1
sample_2
sample_3
sample_1
sample_2
sample_3
(C)
MDA-MB-231
Treatment
Treatment
0 mmHg
11.6 mmHg
SLCO4A1
PPP1R3B
SNAI1
VGLL3
RASSF1
BIRC3
SGK1
GEM
TNFAIP3
FOXC1
IL6R
DYRK3
MAFF
ODC1
MYC
TRIB1
JUN
KDM6B
LOC102724428
ATF3
DUSP1
GADD45B
ID2
UPP1
LINC00973
RRAD
CEBPB
TPRA1
RHOB
C11orf96
1
0.5
0
−0.5
−1
sample_1
sample_2
sample_3
sample_4
sample_5
sample_6
sample_1
sample_2
sample_3
sample_4
sample_5
sample_6
(D)
HepG2/Hep3B
Cell line
Treatment
Cell line
HepG2
Hep3B
Treatment
control
compressed
RASD1
FAM110C
INHBB
TMEM37
VEGFA
SERPINE2
SYT7
S100A11
LGALS1
PDGFB
NDRG1
CP
ANGPTL4
SEMA3G
TGM2
LSP1
PLSCR4
ADSS1
VCAN
TNS4
VNN1
AXL
STC2
TMEM45B
FAM13A
AZGP1
APOL1
ITIH3
PCK1
ISM2
1.5
1
0.5
0
−0.5
−1
−1.5
sample_1
sample_2
sample_1
sample_2
sample_1
sample_2
sample_1
sample_2

**Figure 1. Mechanical compression induces widespread transcriptional remodeling across cancer cell types.** **(A)** Strip plot showing the distribution of log2 fold changes for differentially expressed genes (DEGs; adjusted $P < 0.05$, $|log2FC| \geq 1$) in breast cancer (MDA-MB-231; 154 upregulated, 25 downregulated), hepatocellular carcinoma (HepG2 and Hep3B; 326 upregulated, 29 downregulated), and pancreatic cancer (MIA PaCa-2; 235 upregulated, 39 downregulated) cells subjected to mechanical compression. Each dot represents a single DEG. **(B-D)** Heatmaps of the top differentially expressed genes in **(B)** MIA PaCa-2 cells under 4 mmHg compression for 16 hours (n = 3 biological replicates per condition), **(C)** MDA-MB-231 cells under 11.6 mmHg compression (n = 6 biological replicates per condition), and **(D)** HepG2 and Hep3B cells under confined growth conditions (n = 2 biological replicates per condition per cell line). Color scale represents row-scaled normalized expression values (z-scores). Hierarchical clustering was performed. Treatment conditions are indicated by annotation bars (yellow: control/0 Pa; purple: compressed). In **(D)**, cell line identity is additionally annotated (green: HepG2; purple: Hep3B).

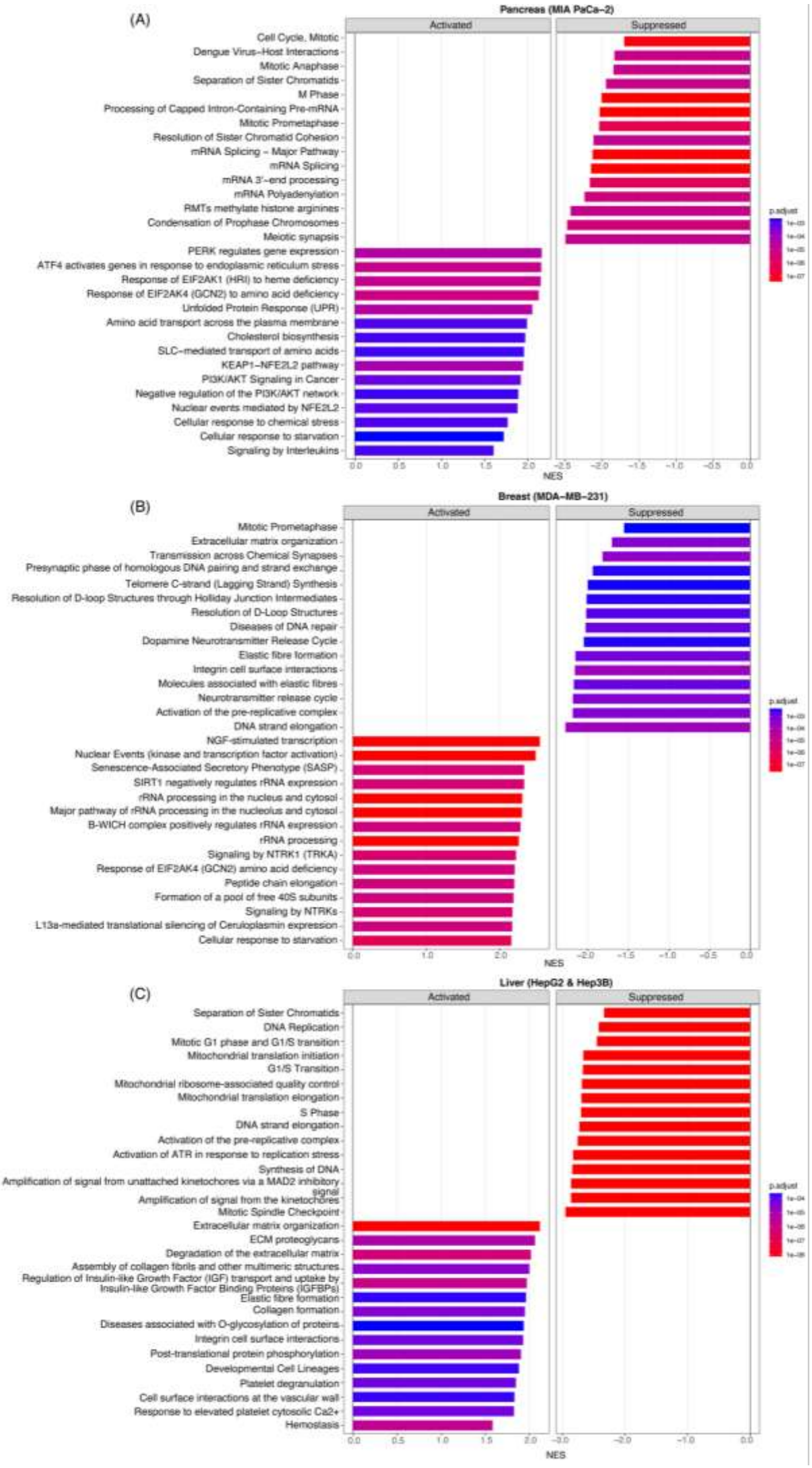

(A)
Pancreas (MIA PaCa−2)
Activated
Suppressed
Cell Cycle, Mitotic
Dengue Virus−Host Interactions
Mitotic Anaphase
Separation of Sister Chromatids
M Phase
Processing of Capped Intron−Containing Pre−mRNA
Mitotic Prometaphase
Resolution of Sister Chromatid Cohesion
mRNA Splicing − Major Pathway
mRNA Splicing
mRNA 3'−end processing
mRNA Polyadenylation
RMTs methylate histone arginines
Condensation of Prophase Chromosomes
Meiotic synapsis
PERK regulates gene expression
ATF4 activates genes in response to endoplasmic reticulum stress
Response of EIF2AK1 (HRI) to heme deficiency
Response of EIF2AK4 (GCN2) to amino acid deficiency
Unfolded Protein Response (UPR)
Amino acid transport across the plasma membrane
Cholesterol biosynthesis
SLC−mediated transport of amino acids
KEAP1−NFE2L2 pathway
PI3K/AKT Signaling in Cancer
Negative regulation of the PI3K/AKT network
Nuclear events mediated by NFE2L2
Cellular response to chemical stress
Cellular response to starvation
Signaling by Interleukins
0.0 0.5 1.0 1.5 2.0
−2.5 −2.0 −1.5 −1.0 −0.5 0.0
NES
p.adjust
1e−03
1e−04
1e−05
1e−06
1e−07
(B)
Breast (MDA−MB−231)
Activated
Suppressed
Mitotic Prometaphase
Extracellular matrix organization
Transmission across Chemical Synapses
Presynaptic phase of homologous DNA pairing and strand exchange
Telomere C−strand (Lagging Strand) Synthesis
Resolution of D−loop Structures through Holliday Junction Intermediates
Resolution of D−Loop Structures
Diseases of DNA repair
Dopamine Neurotransmitter Release Cycle
Elastic fibre formation
Integrin cell surface interactions
Molecules associated with elastic fibres
Neurotransmitter release cycle
Activation of the pre−replicative complex
DNA strand elongation
NGF−stimulated transcription
Nuclear Events (kinase and transcription factor activation)
Senescence−Associated Secretory Phenotype (SASP)
SIRT1 negatively regulates rRNA expression
rRNA processing in the nucleus and cytosol
Major pathway of rRNA processing in the nucleolus and cytosol
B−WICH complex positively regulates rRNA expression
rRNA processing
Signaling by NTRK1 (TRKA)
Response of EIF2AK4 (GCN2) amino acid deficiency
Peptide chain elongation
Formation of a pool of free 40S subunits
Signaling by NTRKs
L13a−mediated translational silencing of Ceruloplasmin expression
Cellular response to starvation
0.0 1.0 2.0
−2.0 −1.5 −1.0 −0.5 0.0
NES
p.adjust
1e−03
1e−04
1e−05
1e−06
1e−07
(C)
Liver (HepG2 & Hep3B)
Activated
Suppressed
Separation of Sister Chromatids
DNA Replication
Mitotic G1 phase and G1/S transition
Mitochondrial translation initiation
G1/S Transition
Mitochondrial ribosome−associated quality control
Mitochondrial translation elongation
S Phase
DNA strand elongation
Activation of the pre−replicative complex
Activation of ATR in response to replication stress
Synthesis of DNA
Amplification of signal from unattached kinetochores via a MAD2 inhibitory signal
Amplification of signal from the kinetochores
Mitotic Spindle Checkpoint
Extracellular matrix organization
ECM proteoglycans
Degradation of the extracellular matrix
Assembly of collagen fibrils and other multimeric structures
Regulation of Insulin−like Growth Factor (IGF) transport and uptake by Insulin−like Growth Factor Binding Proteins (IGFBPs)
Elastic fibre formation
Collagen formation
Diseases associated with O−glycosylation of proteins
Integrin cell surface interactions
Post−translational protein phosphorylation
Developmental Cell Lineages
Platelet degranulation
Cell surface interactions at the vascular wall
Response to elevated platelet cytosolic Ca2+
Hemostasis
0.0 0.5 1.0 1.5 2.0
−3.0 −2.0 −1.0 0.0
NES
p.adjust
1e−04
1e−05
1e−06
1e−07
1e−08

**Figure 2. Gene set enrichment analysis reveals tumor type-specific pathway activation and conserved proliferative suppression under mechanical compression. (A-C)** GSEA results using Reactome pathway annotations for **(A)** MIA PaCa-2 (pancreatic), **(B)** MDA-MB-231 (breast), and **(C)** HepG2/Hep3B (hepatocellular carcinoma) cells subjected to mechanical compression. Bar plots display the top 15 activated (left) and top 15 suppressed (right) pathways ranked by normalized enrichment score (NES). Bar color indicates adjusted P-value (Benjamini–Hochberg correction), with warmer colors (red/magenta) denoting higher statistical significance and cooler colors (blue) denoting comparatively lower significance. Only pathways with adjusted $P < 0.05$ are shown. GSEA was performed on the full ranked gene list (by log2 fold change) from DESeq2 analysis without applying fold-change cutoffs.

## Cross-tumor comparison reveals minimal gene- and pathway-level overlap across tumor models

To evaluate the extent of transcriptional convergence across tumor types, we compared differentially expressed genes (DEGs) under compression across pancreatic, breast and liver cancer models (**Fig. 3**). Projection of the most significant DEGs from each dataset onto a unified gene matrix enabled direct visualization of their regulation patterns (**Fig. 3A**). This comparative mapping revealed that most highly regulated genes were restricted to a single tumor type, with limited overlap between models. Quantitative assessment using UpSet analysis confirmed this observation (**Fig. 3B**). A total of 228 pancreas-specific, 144 breast-specific and 321 liver-specific genes were uniquely regulated under compression. While 23 DEGs were shared between breast and pancreatic cells, 22 between pancreatic and liver cells, and 11 between breast and liver cells, only a single gene—*FOS*—was commonly regulated across all three tumor types. FOS was consistently upregulated in pancreatic (LFC = 1.32), breast (LFC = 2.30) and liver (LFC = 1.54) cancer cells. As an immediate early gene and core component of the AP-1 transcriptional complex, which also includes JUN, FOS represents a canonical stress-responsive transcription factor activated downstream of diverse signaling inputs. Although present in all datasets, FOS is absent from the top-20 gene visualization in Fig. 1, because it ranked lower by adjusted p-value (93rd in breast, 178th in liver, and 242nd in pancreas).

The breast–pancreas overlap (23 genes) was dominated by immediate early and stress-response regulators, including *JUN, ATF3, EGR1, EGR3, CEBPB, DDIT3, GADD45A, MAFF, TRIB1*, and *ZFP36*, together with inflammatory mediators such as *CXCL8, CXCL2,* and *IL6R*, reflecting activation of shared transcriptional stress programs. However, several genes within this overlap showed discordant regulation, highlighting tumor-specific integration of these signals. For example, *ID2* was strongly upregulated in breast cancer cells (LFC = 3.31) but downregulated in pancreatic cells (LFC = −3.04).

The liver–pancreas overlap (22 genes) was enriched for metabolic and extracellular signaling regulators, including *VEGFA, ANGPTL4, ENO2, NDRG1, L1CAM*, and *KLF4*, suggesting partial convergence in metabolic and microenvironmental adaptation. Notably, *CDKN1A (p21)* was upregulated in both liver (LFC = 1.29) and pancreatic cells (LFC = 3.54), linking compression responses to cell cycle regulation and stress-induced growth arrest. In contrast, the breast–liver overlap (11 genes) was comparatively limited and included several discordantly regulated transcripts, such as *SGK1, SLCO4A1,* and *NGFR*, reinforcing the overall minimal convergence at the single gene level.

Given this restricted overlap at the gene level, we next examined whether convergence might emerge at the level of biological pathways, where distinct genes can participate in shared functional programs. Intersection analysis of significantly enriched Reactome pathways

demonstrated that most pathways remained tumor-specific (**Fig. 3C**). Nevertheless, pairwise pathway overlaps (60 breast–pancreas, 51 liver–pancreas, and 41 breast–liver pathways) substantially exceeded gene-level intersections, suggesting that functional convergence occurs more strongly at the pathway level. Only five pathways were shared across breast, liver, and pancreatic cancer cells: deposition of new CENPA-containing nucleosomes at the centromere, nucleosome assembly, amyloid fiber formation, extracellular matrix (ECM) organization, and interleukin-4/interleukin-13 signaling. These shared pathways represent distinct biological axes relevant to tumor adaptation. Deposition of new CENPA-containing nucleosomes and nucleosome assembly reflect chromatin organization and centromere maintenance processes linked to mitotic regulation. Amyloid fiber formation is associated with proteostasis and protein aggregation under cellular stress. ECM organization encompasses collagen remodeling and integrin-mediated adhesion dynamics that influence tumor–stroma interactions. Interleukin-4/interleukin-13 signaling represents inflammatory cytokine pathways implicated in immune modulation and microenvironmental adaptation.

To determine whether these shared pathways were regulated in a similar manner across tumor types, we compared their normalized enrichment scores (NES) (**Fig. 3D**). This heatmap representation captures both magnitude and directionality of pathway enrichment under compression. Deposition of new CENPA-containing nucleosomes and nucleosome assembly were enriched in breast cancer cells but suppressed in liver and pancreatic models, consistent with the repression of cell cycle–associated programs observed in those tumor types. Amyloid fiber formation was enriched in breast and liver cells but suppressed in pancreatic cells. ECM organization was strongly enriched in liver cancer and moderately enriched in pancreatic cells, aligning with the prominent matrix remodeling signature identified in the liver GSEA analysis. In contrast, interleukin-4/interleukin-13 signaling was enriched across all three tumor types, representing the only uniformly activated pathway under compression.

Gene–pathway network projection further demonstrated that, despite nominal pathway overlap, the underlying gene composition differed substantially across tumor contexts (**Fig. 3E**). In this network representation, pathways are shown as category-labeled nodes connected to contributing genes, with node coloring and edge weighting reflecting tumor-specific contributions and mean $\log_2$ fold change. The IL-4/IL-13 signaling node includes genes such as *CDKN1A* and *VEGFA*, illustrating how shared pathways integrate genes involved in both inflammatory signaling and cell cycle regulation. Chromatin-associated nodes contain clusters of histone genes (*H2AC, H2BC*, and *H4C* families), which were predominantly downregulated across models. The ECM node incorporates collagen, matrix metalloproteinase, and integrin family members, and halo-ring visualization indicates that this pathway is largely driven by liver-specific transcriptional contributions, whereas IL-4/IL-13 signaling receives contribution from all three tumor types.

Collectively, these findings indicate that cross-tumor convergence of compression-induced responses is limited at both the gene and pathway levels. Even where pathway overlap exists, differences in directionality, gene composition, and relative contribution highlight tumor-context–specific regulatory architecture rather than a single conserved mechanotranscriptional core.

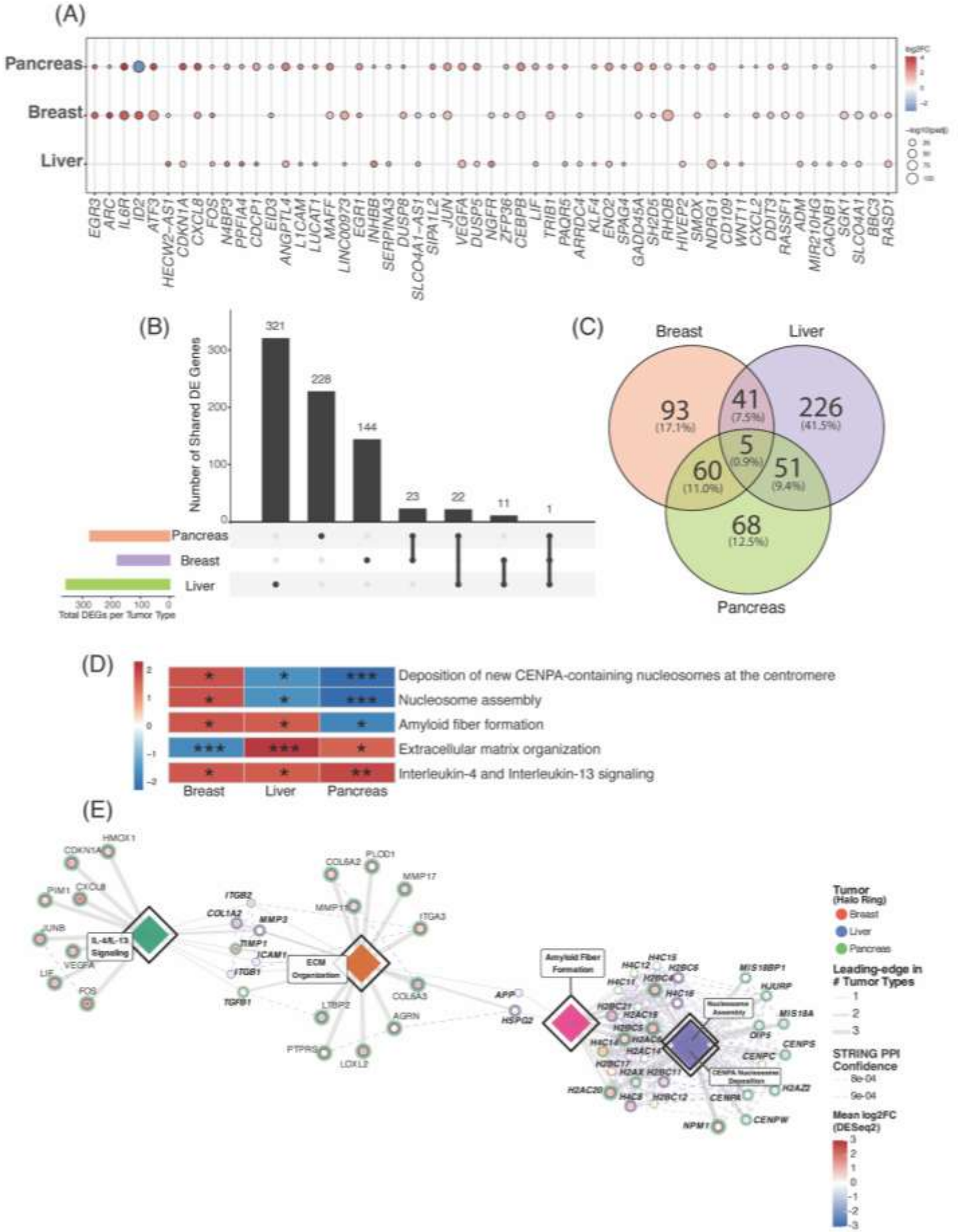

(A)
Pancreas
Breast
Liver
EGR3
ARC
IL6R
ID2
ATF3
HECW2-AS1
CDKN1A
CXCL8
FOS
N4BP3
PPFIA4
CDCP1
EID3
ANGPTL4
L1CAM
LUCAT1
MAFF
LINC00973
EGR1
INHBB
SERPINA3
DUSP8
SLCO4A1-AS1
SIPA1L2
JUN
VEGFA
DUSP5
NGFR
ZFP36
CEBPB
LIF
TRIB1
PAQR5
ARRDC4
KLF4
ENO2
SPAG4
GADD45A
SH2D5
RHOB
HIVEP2
SMOX
NDRG1
CD109
WNT11
CXCL2
DDIT3
RASSF1
ADM
MIR210HG
CACNB1
SGK1
SLCO4A1
BBC3
RASD1
(B)
Number of Shared DE Genes
321
228
144
23
22
11
1
Pancreas
Breast
Liver
Total DEGs per Tumor Type
(C)
Breast
Liver
Pancreas
93
(17.1%)
41
(7.5%)
226
(41.5%)
5
(0.9%)
60
(11.0%)
51
(9.4%)
68
(12.5%)
(D)
Deposition of new CENPA-containing nucleosomes at the centromere
Nucleosome assembly
Amyloid fiber formation
Extracellular matrix organization
Interleukin-4 and Interleukin-13 signaling
Breast
Liver
Pancreas
(E)
IL-4/IL-13 Signaling
ECM Organization
Amyloid Fiber Formation
Nucleosome Assembly
CENPA Nucleosome Deposition
Tumor (Halo Ring)
Breast
Liver
Pancreas
Leading-edge in # Tumor Types
STRING PPI Confidence
Mean log2FC (DESeq2)

**Figure 3. Cross-tumor comparison reveals limited gene-level overlap but identifies shared pathway programs under mechanical compression. (A)** Bubble plot displaying the top 20 most significant DEGs per tumor type projected onto a unified gene matrix. Each dot represents a gene's differential expression in a given tumor type; dot color indicates log2 fold change (red: upregulated; blue: downregulated) and dot size reflects statistical significance (−log10 adjusted P-value). Only genes meeting significance thresholds (adjusted $P < 0.05$, $|log2FC| \geq 1$) in at least one tumor type are shown. **(B)** UpSet plot quantifying the number of shared and tumor-specific DEGs across breast, liver, and pancreatic models. Horizontal bars indicate total DEGs per tumor type; vertical bars indicate the number of DEGs unique to each intersection. **(C)** Venn diagram of significantly enriched Reactome pathways (GSEA, adjusted $P < 0.05$) shared across tumor types. Numbers and percentages indicate the count and proportion of total unique pathways in each intersection. **(D)** Heatmap of normalized enrichment scores (NES) for the five Reactome pathways enriched across all three tumor types. Color scale represents NES magnitude and directionality (red: activated under compression; blue: suppressed). Asterisks denote statistical significance (*Padj < 0.05; **Padj < 0.01; ***Padj < 0.001). Pathways are grouped by functional category (color-coded sidebar: purple, chromatin and epigenetics; pink, development and differentiation; orange, ECM and cell adhesion; green, inflammation and immune response). **(E)** Gene–pathway network visualization of the five shared pathways and their contributing leading-edge genes. Diamond nodes represent pathways, colored by functional category. Circular gene nodes are colored by mean log2 fold change across tumor types in which the gene is a leading-edge member (red: upregulated; blue: downregulated). Halo rings indicate which tumor type(s) contributed each gene (red: breast; blue: liver; green: pancreas). Edge thickness between gene nodes reflects STRING protein–protein interaction confidence score. Node border thickness indicates the number of tumor types (1–3) in which the gene appeared in the leading edge.

## Compression-induced transcriptional programs are largely independent of pre-existing molecular alterations

Given the limited overlap between cancer cell types observed at both gene and pathway levels, we next asked whether the tumor-specific compression responses might be shaped by the intrinsic genomic landscape of each cancer cell line. To address this, we cross-referenced compression-induced DEGs with pre-existing somatic mutations, copy number alterations (CNAs), and abnormal baseline expression annotated in DepMap/CCLE (**Fig. 4**). Across all tumor types, most compression-responsive genes showed no associated genomic alteration (**Fig. 4A**). Specifically, 92.7% of DEGs in pancreatic, 98.3% in breast and 88.5% in liver cells were genomically unaltered. Only small fractions of DEGs overlapped with genomic alterations. In pancreatic cells, 20 altered DEGs were identified, including nine genes with somatic mutations and eleven genes showing abnormal baseline expression. In breast cancer cells, only three altered DEGs were detected, all carrying somatic mutations (LURAP1L, DIO2, and LRP1B). Liver cancer cells showed the largest number of altered DEGs (41 genes), largely dominated by abnormal baseline expression events (36 genes), with only two somatic mutations and three CNAs. The comparatively higher alteration rate in liver models was driven almost entirely by abnormal baseline expression, consistent with the known tissue-specific expression profiles of hepatocellular carcinoma cell lines in CCLE, rather than by somatic mutations or CNAs.

Among the compression-responsive DEGs shared across tumor types (**Fig. 3**), key genes including FOS—the only DEG common to all three models—as well as JUN, ATF3, CEBPB, GADD45A, VEGFA, ANGPTL4, ENO2, and NDRG1 were genomically unaltered in every tumor type in which they were differentially expressed, indicating that these canonical stress-responsive transcription factors and metabolic regulators are activated by mechanical compression independently of pre-existing genomic alterations.

To visualize the relationship between compression responsiveness and pre-existing alteration status across the full transcriptome, we generated volcano plots in which all genes from the DESeq2 analysis were plotted by their compression-induced fold change (x-axis) and statistical significance (y-axis), with each gene colored according to its genomic alteration

status in DepMap/CCLE (**Fig. 4B**). Genes exceeding both significance thresholds (padj < 0.05 and |log2FC| >= 1) that carried no pre-existing alteration are shown in mint green, representing the vast majority of compression-responsive DEGs. The small number of DEGs that also harbored a pre-existing somatic mutation, CNA, or abnormal baseline expression are highlighted in red and labeled by gene name. These altered DEGs were distributed across the fold-change spectrum and did not preferentially cluster among the most strongly regulated transcripts. Non-responsive genes carrying pre-existing alterations (pastel orange) were scattered throughout the sub-threshold region, further indicating that genomic alterations alone do not predispose genes to compression responsiveness. Across all three tumor types, the significant zone of each volcano was dominated by genomically unaltered genes, reinforcing that mechanical compression acts as the primary driver of transcriptional reprogramming rather than amplifying pre-existing genetic vulnerabilities.

To determine whether mutational convergence might nevertheless emerge at the pathway level, we performed over-representation analysis (ORA) of Reactome pathways enriched among genes harboring somatic mutations and compared these mutation-associated pathways with compression-induced programs identified by GSEA (**Suppl. Fig. 1**). In pancreatic cells, mutation-enriched pathways were dominated by glycosylation processes, lipophagy, chylomicron assembly, and PLC-mediated signaling. Notably, while mechanical compression in pancreatic tumors activated PERK-regulated gene expression and unfolded protein response (UPR) pathways (**Fig. 2A**), the pre-existing glycosylation and proteostatic defects encoded in the mutational background suggest that pancreatic tumors may be uniquely primed for protein folding stress, and that mechanical compression further exacerbates this pre-existing proteostatic vulnerability rather than initiating it de novo. In breast cancer cells, mutation-enriched pathways included NOTCH receptor processing, O-glycosylation defects, TP53-regulated transcriptional programs, and integrin-associated signaling. Under mechanical compression, breast tumors activated NRF2-stimulated transcription while suppressing ECM organization and mitotic progression (**Fig. 2B**)—a particularly striking divergence given that ECM organization was also a feature of the mutational background, suggesting that mechanical force may override or counteract mutation-driven ECM programs in breast tumors. In liver models, mutation-associated pathways prominently involved RAS downstream signaling, PDGF and VEGFR pathways, RHO GTPase signaling, and metabolic processes, while mechanical compression instead drove strong activation of collagen formation and ECM remodeling alongside broad suppression of cell cycle progression and DNA synthesis (**Fig. 2C**). The convergence of collagen-related pathways in both the mutational and compression-responsive contexts of liver tumors suggests this pathway may be especially central to liver tumor mechanobiology, even as the broader mutational and compression signatures remain distinct. Importantly, with the exception of these select pathway-level overlaps, mutation-driven pathways were largely distinct from the compression-responsive programs described in **Fig. 2**, which were characterized by activation of integrated stress response networks, ECM remodeling, transcriptional and translational adaptation, and coordinated suppression of cell cycle machinery. No consistent overlap was observed between mutation-enriched and compression-enriched functional programs across tumor types. The context-dependent responses observed across tumor models therefore reflect differential mechanoadaptive integration rather than intrinsic mutational bias.

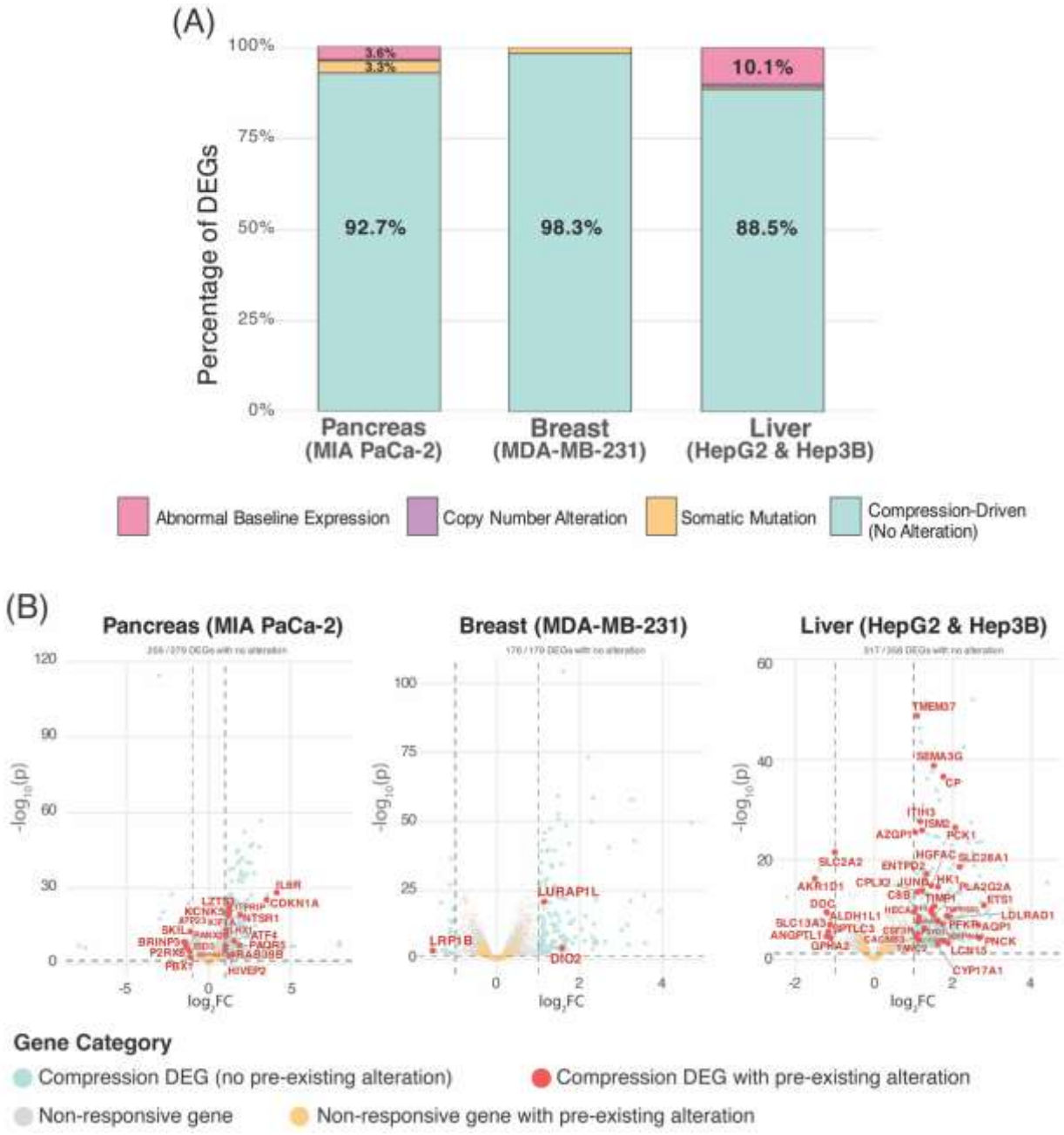



**Figure 4. Compression-induced transcriptional responses are largely independent of pre-existing genomic alterations. (A)** Stacked bar plots showing the proportion of compression-responsive DEGs (adjusted P < 0.05, |log2FC| >= 1) overlapping with pre-existing genomic alterations in pancreatic (MIA PaCa-2), breast (MDA-MB-231), and liver (HepG2 and Hep3B) cancer cell lines. Alteration categories include somatic mutations, copy number alterations (CNAs), and abnormal baseline expression, defined as expression values exceeding +/-2 standard deviations from the pan-cancer mean across CCLE cell lines. Genes with no annotated alteration are classified as compression driven. Percentages indicate the fraction of DEGs in each category. **(B)** Volcano plots displaying the full DESeq2 differential expression results (compressed vs. control) for each tumor type. Each point represents a gene, plotted by log2 fold change (x-axis) and -log10 adjusted P-value (y-axis). Dashed lines indicate significance thresholds (adjusted P = 0.05; |log2FC| = 1). Genes are colored by their pre-existing genomic alteration status in DepMap/CCLE: grey, non-responsive genes with no alteration; pastel orange, non-responsive genes harboring a pre-existing alteration; mint green, compression-responsive DEGs with no pre-existing alteration; red, compression-responsive DEGs carrying a pre-existing somatic mutation, CNA, or abnormal baseline expression. Only DEGs with pre-existing alterations (red) are labeled by gene name. Genomic alteration data were obtained from the DepMap portal (release 24Q4) and the Cancer Cell Line Encyclopedia (CCLE).

**Compression-associated transcriptional signatures are detectable in-patient tumors and associate with clinical outcome**

To determine whether the compression-induced transcriptional programs identified *in vitro* are recapitulated in human tumors, we projected our *in vitro* compression signatures onto bulk RNA-seq data from The Cancer Genome Atlas (TCGA) using single-sample gene set enrichment analysis (ssGSEA) (**Fig. 5**). For each cancer type, the compression-responsive DEGs (adjusted P < 0.05, |log2FC| >= 1) were split into upregulated and downregulated gene sets based on their direction of change under compression *in vitro*. Each TCGA patient sample was then scored against these gene sets using ssGSEA, which ranks all ~20,000 expressed genes in a patient's transcriptome and computes an enrichment score reflecting how coordinately the signature genes are expressed relative to the full transcriptomic background. The final compression score for each patient was calculated as ssGSEA(upregulated genes) minus ssGSEA(downregulated genes), such that a higher score indicates greater transcriptional similarity to the mechanically compressed state observed *in vitro*. Importantly, each TCGA cohort was scored using its cancer-matched *in vitro* signature: breast compression DEGs for TCGA-BRCA, liver DEGs for TCGA-LIHC, and pancreatic DEGs for TCGA-PAAD. To ensure robustness, three additional scoring methods were computed in parallel (mean ratio, z-score, and weighted signature score; see Methods); ssGSEA was selected as the primary metric given its established use in the field and strong concordance with the alternative methods (31). Normal tissue comparators included both TCGA adjacent normal tissues and non-diseased tissues from the Genotype-Tissue Expression (GTEx) project, and analyses were restricted to treatment-naive patients with no prior radiation or targeted therapy.

Comparison of compression scores across tumor and normal tissues revealed tumor-type-specific patterns (**Fig. 5A**). In pancreatic cancer, compression scores were uniformly high across tumors and remained elevated relative to normal tissues. In breast cancer, tumors exhibited modestly elevated compression scores relative to GTEx and adjacent normal tissues. In liver cancer, tumor samples showed a clear increase in compression score compared to normal liver controls. Collectively, these findings demonstrate that the transcriptional programs activated by mechanical compression in vitro are detectable in patient tumors and are preferentially enriched in malignant relative to normal tissues, particularly in liver and pancreatic cancers.

We next examined whether compression-associated transcriptional activity correlates with disease progression using American Joint Committee on Cancer (AJCC) pathological stage (**Fig. 5B**). In pancreatic cancer, compression scores remained consistently elevated across stages with limited variation. In breast cancer, compression scores showed a modest decline with advancing stage. In liver cancer, compression scores increased progressively from early to later stages, consistent with enrichment of the compression signature during tumor advancement. These data suggest that the relationship between compression-associated transcriptional activity and disease progression is tumor-type dependent, with the most pronounced stage association observed in liver cancer.

To assess prognostic relevance, patients were stratified into high and low compression-score groups by median split and analyzed using Kaplan-Meier survival curves (**Fig. 5C**). In breast cancer, compression score was not significantly associated with overall survival (log-rank p = 0.17; HR = 0.53 [0.09-3.04]). In contrast, high compression scores were associated with significantly reduced survival in liver cancer (p = 0.0064; HR = 2.21 [0.87-5.58]) and pancreatic

cancer (p = 0.0047; HR = 34.55 [1.49-800.88]). These findings indicate that elevated compression-associated transcriptional activity — as measured by the correspondence between a patient's tumor transcriptome and the in vitro compression response — correlates with poorer clinical outcomes in liver and pancreatic malignancies. To determine whether the compression signature provides prognostic information independently of established clinical variables, we performed multivariate Cox proportional hazards regression adjusting for age, gender, tumor stage, histologic grade (where applicable), radiation therapy, residual tumor status, and targeted molecular therapy (**Suppl. Fig. 2**). In pancreatic cancer, the compression score exhibited a markedly elevated hazard ratio (HR = 6.73 [0.77-59.08]), suggesting a potential strong adverse association with survival. However, the wide confidence interval reflects the limited sample size of the treatment-naive pancreatic subgroup and precludes definitive conclusions regarding its independent prognostic value. In contrast, the compression score was not associated with survival in breast cancer (HR = 0.96 [0.22-4.10]). Similarly, in liver cancer, although a modest increase in hazard was observed (HR = 1.18 [0.36-3.90]), this effect was not statistically significant after adjustment for clinical covariates.

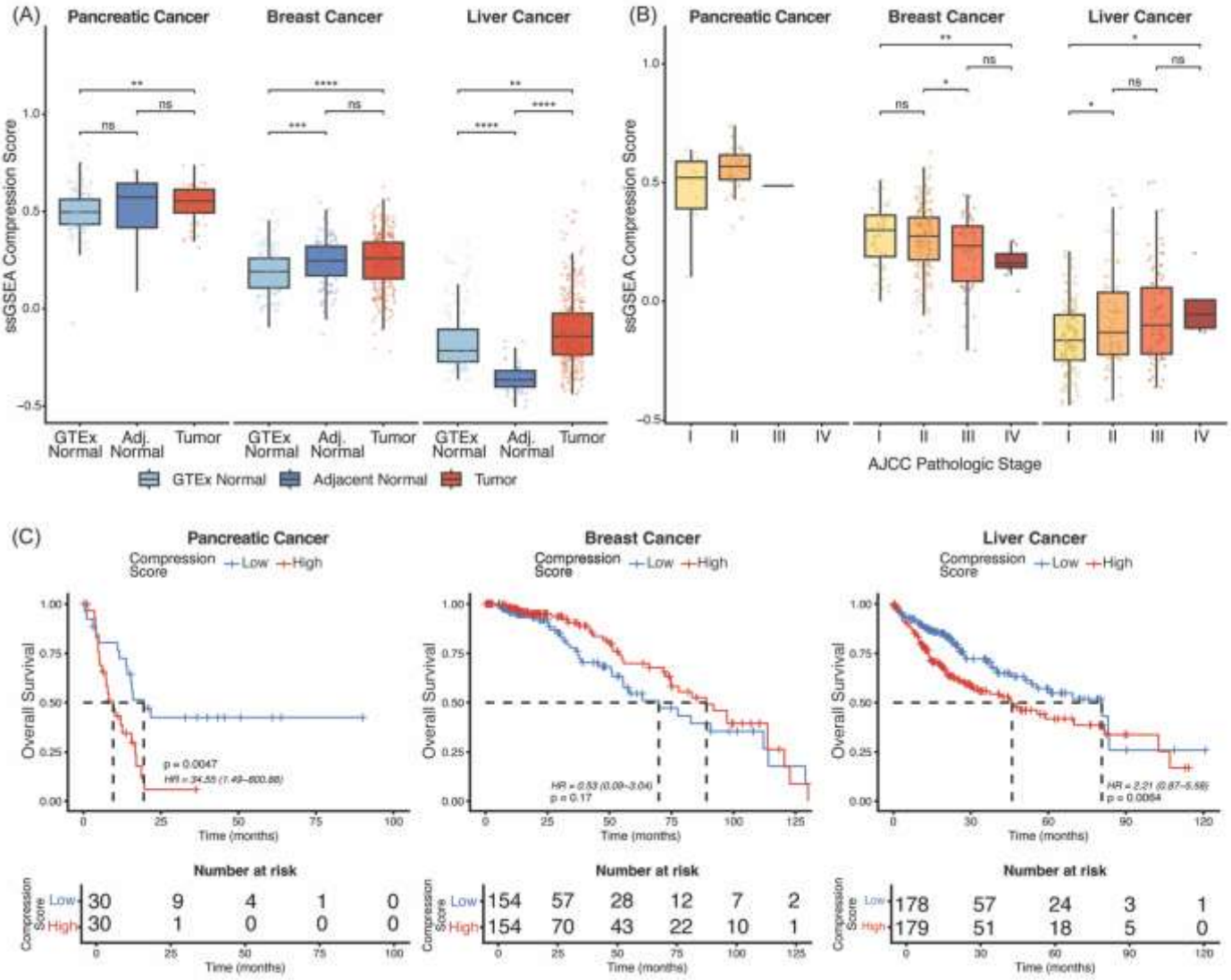



**Figure 5. Clinical relevance of the mechanical compression transcriptional signature in TCGA patient tumors.** Compression signature scores were computed by single-sample gene set enrichment analysis (ssGSEA) using differentially expressed genes (padj < 0.05, |log2FC| ≥ 1) from in vitro compression experiments matched to each cancer type. Analyses were restricted to treatment-naive patients (no prior radiation or targeted molecular therapy). Normal tissue comparators include GTEx non-diseased tissues and TCGA adjacent normal samples. All expression data were uniformly reprocessed through the STAR–RSEM pipeline (UCSC Xena Toil Hub). **(A)** Compression signature scores in normal tissues and tumors across pancreatic (PAAD), breast (BRCA), and liver (LIHC) cancer. Boxplots display median and interquartile range; individual samples are shown as jittered points. Pairwise comparisons were performed using two-sided Wilcoxon rank-sum tests. Significance levels: ns, not significant; *p < 0.05; **p < 0.01; ***p < 0.001; ****p < 0.0001. **(B)** Compression signature scores stratified by AJCC pathologic stage (I–IV) among treatment-naive tumors. Pairwise comparisons between consecutive stages and between Stage I and Stage IV were assessed by Wilcoxon rank-sum tests. Significance annotations as in (A). **(C)** Kaplan–Meier overall survival curves for treatment-naive patients stratified by median compression score (high vs low) within each cancer type. P-values are from log-rank tests. Hazard ratios (HR) and 95% confidence intervals were estimated by univariate Cox proportional hazards regression. Number-at-risk tables are shown below each curve. Censored events are indicated by tick marks.

**Compression-induced molecular reprogramming intersects with therapeutic targets in pancreatic cancer**

Given that compression-associated transcriptional signatures showed the strongest prognostic associations in pancreatic cancer, we next investigated whether mechanically responsive genes converge with therapeutic strategies currently under clinical evaluation in PDAC, reasoning that genes enriched in aggressive disease may represent actionable vulnerabilities. To contextualize this within the clinical landscape, we first compiled drugs evaluated in PDAC clinical trials using the Open Targets Platform and classified them according to their highest clinical phase reached and mechanism of action (**Fig. 6A**). Across clinical phases, multiple therapeutic categories are represented in PDAC, including conventional chemotherapy, kinase inhibitors, VEGF/angiogenesis-targeted agents, immunomodulatory drugs, epigenetic regulators, metabolic agents, and pathway-directed therapies. While several categories advance through Phase 2 and Phase 3 trials, only a limited subset progress to Phase 4, where conventional cytotoxic therapies and selected targeted approaches predominate. In contrast, many pathway-directed, immunomodulatory, and epigenetic strategies remain confined to earlier developmental stages. We next assessed whether compression-induced DEGs intersect with these clinically investigated drug classes. Mapping compression-responsive genes to PDAC trial drugs revealed that 56 drugs share gene targets with the compression signature (**Fig. 6B**). Mechanistic classes sharing the largest number of compression-regulated genes (>5 genes) included COX/anti-inflammatory agents (8 genes), antimetabolites and DNA synthesis inhibitors (7 genes), VEGF/angiogenesis-targeted therapies (7 genes), kinase inhibitors (6 genes), and tubulin inhibitors (6 genes). These results indicate substantial overlap between mechanically regulated transcriptional programs and major therapeutic axes currently pursued in PDAC. To further resolve specific drug-gene relationships, we interrogated curated drug-gene interactions using DGIdb 5.0 (**Fig. 7**) (32). Several clinically relevant agents intersected with multiple compression-induced genes. Notably, gemcitabine was linked to compression-responsive genes including *ACSS2* and *SH2D5*. In addition, receptor tyrosine kinase inhibitors (e.g., sunitinib, sorafenib), VEGF-directed therapies (bevacizumab, aflibercept), and mTOR-targeted agents (everolimus, temsirolimus) intersected with compression-regulated genes such as *VEGFA, HMOX1*, and *NOTCH4*, linking compressive stress to signaling networks central to PDAC treatment strategies. The highest-scoring interaction was *TNFRSF9* (DGIdb score 78.3), the target of the agonist antibody urelumab currently in Phase 1 PDAC trials. Importantly, several drugs

shared multiple targets within the compression signature, uggesting coordinated modulation of drug-relevant signaling networks rather than isolated gene-drug associations.

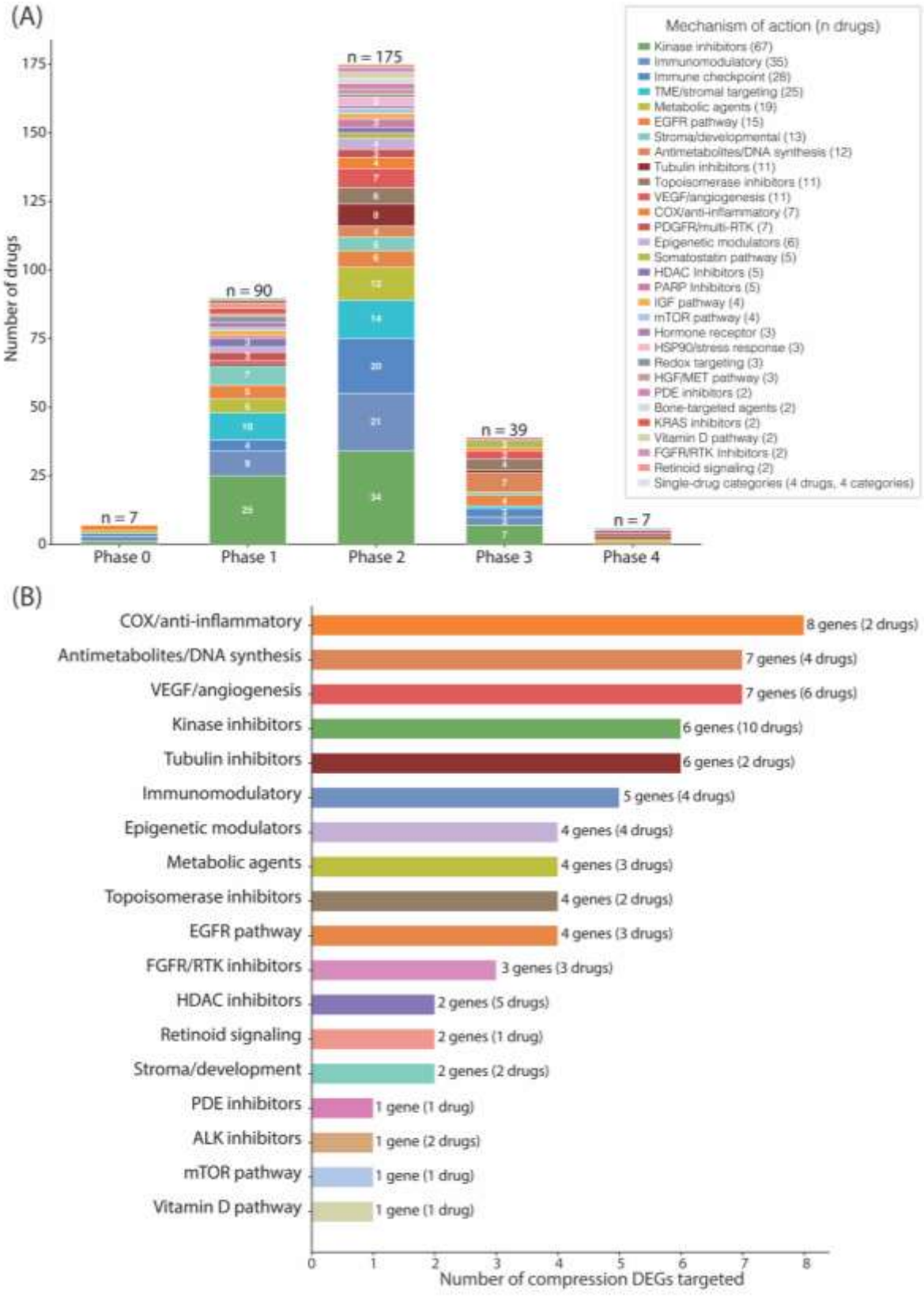

(A)
Number of drugs
n = 7
n = 90
n = 175
n = 39
n = 7
Phase 0
Phase 1
Phase 2
Phase 3
Phase 4
Mechanism of action (n drugs)
Kinase inhibitors (67)
Immunomodulatory (35)
Immune checkpoint (28)
TME/stromal targeting (25)
Metabolic agents (19)
EGFR pathway (15)
Stroma/developmental (13)
Antimetabolites/DNA synthesis (12)
Tubulin inhibitors (11)
Topoisomerase inhibitors (11)
VEGF/angiogenesis (11)
COX/anti-inflammatory (7)
PDGFR/multi-RTK (7)
Epigenetic modulators (6)
Somatostatin pathway (5)
HDAC inhibitors (5)
PARP inhibitors (5)
IGF pathway (4)
mTOR pathway (4)
Hormone receptor (3)
HSP90/stress response (3)
Redox targeting (3)
HGF/MET pathway (3)
PDE inhibitors (2)
Bone-targeted agents (2)
KRAS inhibitors (2)
Vitamin D pathway (2)
FGFR/RTK inhibitors (2)
Retinoid signaling (2)
Single-drug categories (4 drugs, 4 categories)
(B)
COX/anti-inflammatory
8 genes (2 drugs)
Antimetabolites/DNA synthesis
7 genes (4 drugs)
VEGF/angiogenesis
7 genes (6 drugs)
Kinase inhibitors
6 genes (10 drugs)
Tubulin inhibitors
6 genes (2 drugs)
Immunomodulatory
5 genes (4 drugs)
Epigenetic modulators
4 genes (4 drugs)
Metabolic agents
4 genes (3 drugs)
Topoisomerase inhibitors
4 genes (2 drugs)
EGFR pathway
4 genes (3 drugs)
FGFR/RTK inhibitors
3 genes (3 drugs)
HDAC inhibitors
2 genes (5 drugs)
Retinoid signaling
2 genes (1 drug)
Stroma/development
2 genes (2 drugs)
PDE inhibitors
1 gene (1 drug)
ALK inhibitors
1 gene (2 drugs)
mTOR pathway
1 gene (1 drug)
Vitamin D pathway
1 gene (1 drug)
Number of compression DEGs targeted

**Figure 6. Clinical drug landscape of pancreatic cancer and intersection with compression-responsive genes. (A)** Distribution of drugs investigated in pancreatic cancer clinical trials across development phases (Phase 0–4), classified by mechanism of action. Drug–disease associations and trial phases were retrieved from the Open Targets Platform using verified pancreatic cancer disease identifiers (EFO_0002618, MONDO_0005184, EFO_1000044, EFO_0003860, EFO_1000359) with complete pagination across all available records. Each drug was assigned to a single mechanistic category based on its primary mechanism of action annotation. Gemcitabine was reclassified as Phase 4 based on its FDA-approved status for PDAC (Open Targets records Phase 3 from control-arm trial entries). Non-therapeutic agents (bupivacaine, propofol, digoxin, warfarin, omeprazole, bethanechol, epoetin alfa, dexamethasone, mycophenolate mofetil) were excluded. **(B)** Number of compression-responsive differentially expressed genes (padj < 0.05, |log2FC| ≥ 1) targeted by drugs within each mechanistic category. Bar length represents the number of unique compression DEGs targeted; bar labels indicate the number of genes and the number of drugs within each category. Drug–gene interactions were queried via DGIdb 5.0 (GraphQL API) and cross-referenced with the Open Targets PDAC drug list.

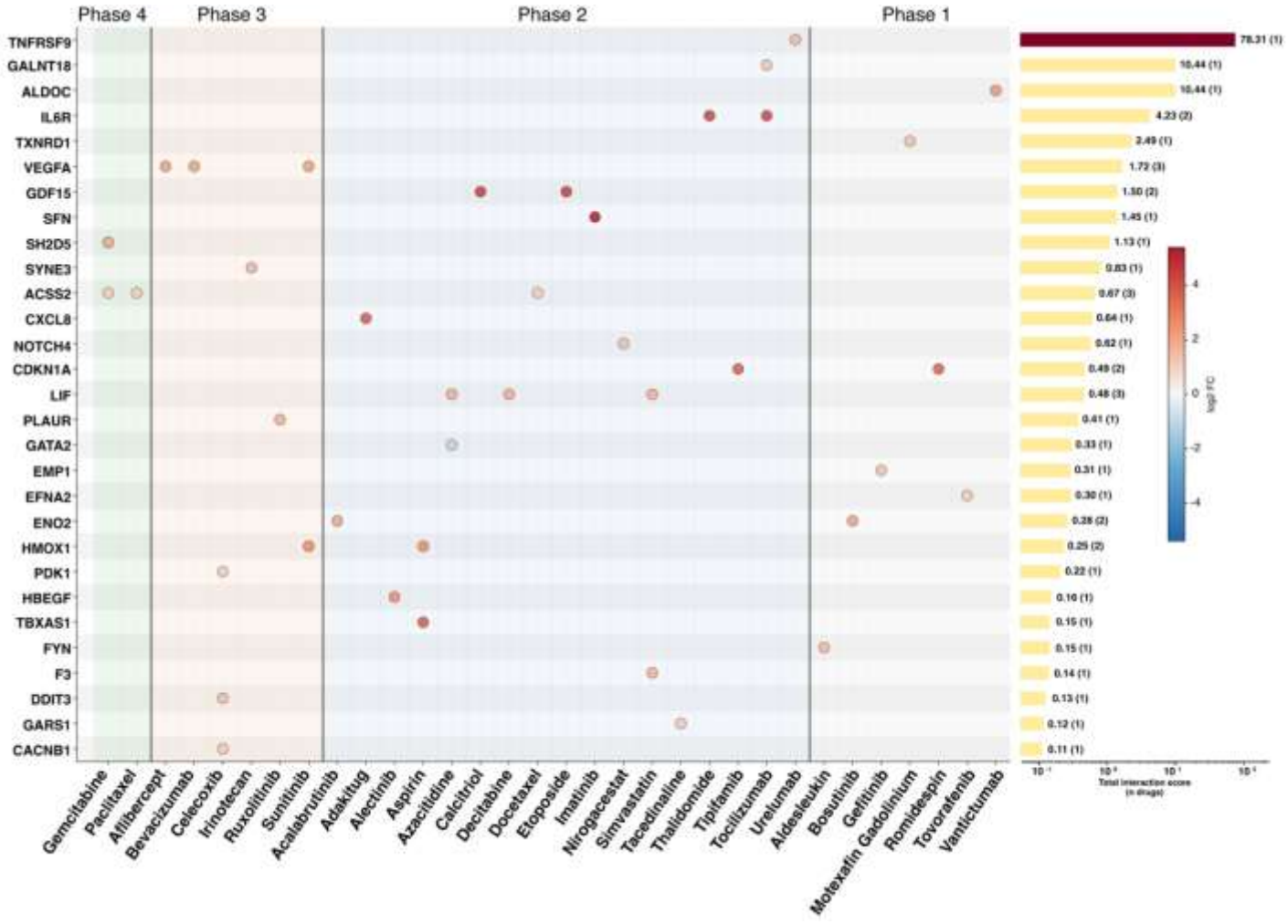



**Figure 7. Drug–gene interaction map of compression-responsive genes and PDAC-investigated therapeutics.** Dot matrix displaying curated interactions between compression-responsive DEGs (rows, ordered by total DGIdb interaction score) and drugs clinically investigated in pancreatic cancer (columns, grouped by highest PDAC-specific trial phase). Dot color indicates the log2 fold change of each gene under compression (red: upregulated; blue: downregulated; diverging colormap centered at zero). Column background shading denotes PDAC clinical trial phase (green: Phase 4; orange: Phase 3; blue: Phase 2; gray: Phase 1). Vertical lines separate phase groups. Right-side horizontal bars show the total DGIdb interaction score per gene (YlOrRd gradient, log10 scale), with the number of interacting drugs in parentheses. Drug–gene interactions were retrieved from DGIdb 5.0 (interaction score ≥ 0.1) and cross-referenced with the Open Targets Platform for PDAC trial phase assignment. Sunitinib phase reflects PDAC adenocarcinoma trials only (excluding pancreatic neuroendocrine tumor indications).

Because many of the implicated therapeutic classes directly depend on cellular metabolic state, including antimetabolites that target nucleotide synthesis, kinase inhibitors regulating nutrient sensing and lipid metabolism, and inflammatory or angiogenic therapies connected to redox and hypoxia responses, we next investigated whether compression induces corresponding metabolic adaptations. We therefore performed LC-MS-based exometabolomic profiling of conditioned media from compressed versus control MIA PaCa-2 cells (**Fig. 8**). Raw peak intensities were acquired across 557 compounds in both positive (231 compounds) and negative (326 compounds) electrospray ionization modes from three biological conditions (Control, Compressed, and cell-free Media; n = 3 per group).

Hierarchical clustering of the 27 metabolites passing significance thresholds across both ionization modes revealed clear separation between compressed and control exometabolic profiles (**Fig. 8A**). Several biologically coherent clusters emerged: sphinganine-phosphate, phospholipids PS(18:0/18:0) and PC(20:3/14:1) grouped together, indicating coordinated sphingolipid and phospholipid remodeling under compression; purine-derived metabolites (1,3-dimethyluric acid, xanthosine) clustered with redox markers (monodehydroascorbate, sulfurous acid); and DNA damage products (thymidine glycol) appeared alongside modified nucleotides. Compound class annotation confirmed that significantly altered metabolites spanned carboxylic acids, fatty acyls, glycerophospholipids, sphingolipids, and purine nucleosides (**Fig. 8B**). ORA analysis against the RaMP metabolite set library identified 14 biologically relevant enriched pathways (**Fig. 8C**), organized around four functional themes: purine nucleotide metabolism (enrichment ratio 38.7, $p = 0.001$), sulfur and redox metabolism (sulfide oxidation to sulfate, cysteine metabolism, methionine and sulfur amino acid metabolism), sphingolipid signaling (sphingolipid catabolism, sphingolipid pathway, ER and Golgi sphingolipid metabolism), and amino acid catabolism (lysine degradation). The most significantly enriched pathway was molybdenum cofactor biosynthesis (enrichment ratio 138.9, $p = 7.91 \times 10^{-5}$), which produces a sulfur-containing cofactor required for redox enzymes involved in oxidative metabolism and xenobiotic detoxification, linking compression-induced metabolic changes to pathways relevant for drug metabolism.

These metabolic alterations also align with and independently validate the transcriptional programs identified by RNA-seq. Purine metabolite depletion corresponds to the activated integrated stress response (*ATF4, ASNS, CHAC1*); sphingolipid remodeling parallels GSEA enrichment of sphingolipid biosynthesis driven by coordinated sub-threshold upregulation of *SPHK1, KDSR*, and *CERS1*; and sulfur/cysteine metabolic pathway enrichment converges with transcriptional activation of the KEAP1-NFE2L2 antioxidant axis (*SLC7A11, GCLC, CTH, TXNRD1*). Together, both analyses support a model in which mechanical compression establishes a coordinated transcriptional and metabolic state that converges with key therapeutic pathways in pancreatic cancer (**Fig. 9**). While these findings do not directly

demonstrate drug resistance, they suggest that mechanical stress may reshape metabolic dependencies and signaling networks in ways that influence therapeutic vulnerability.

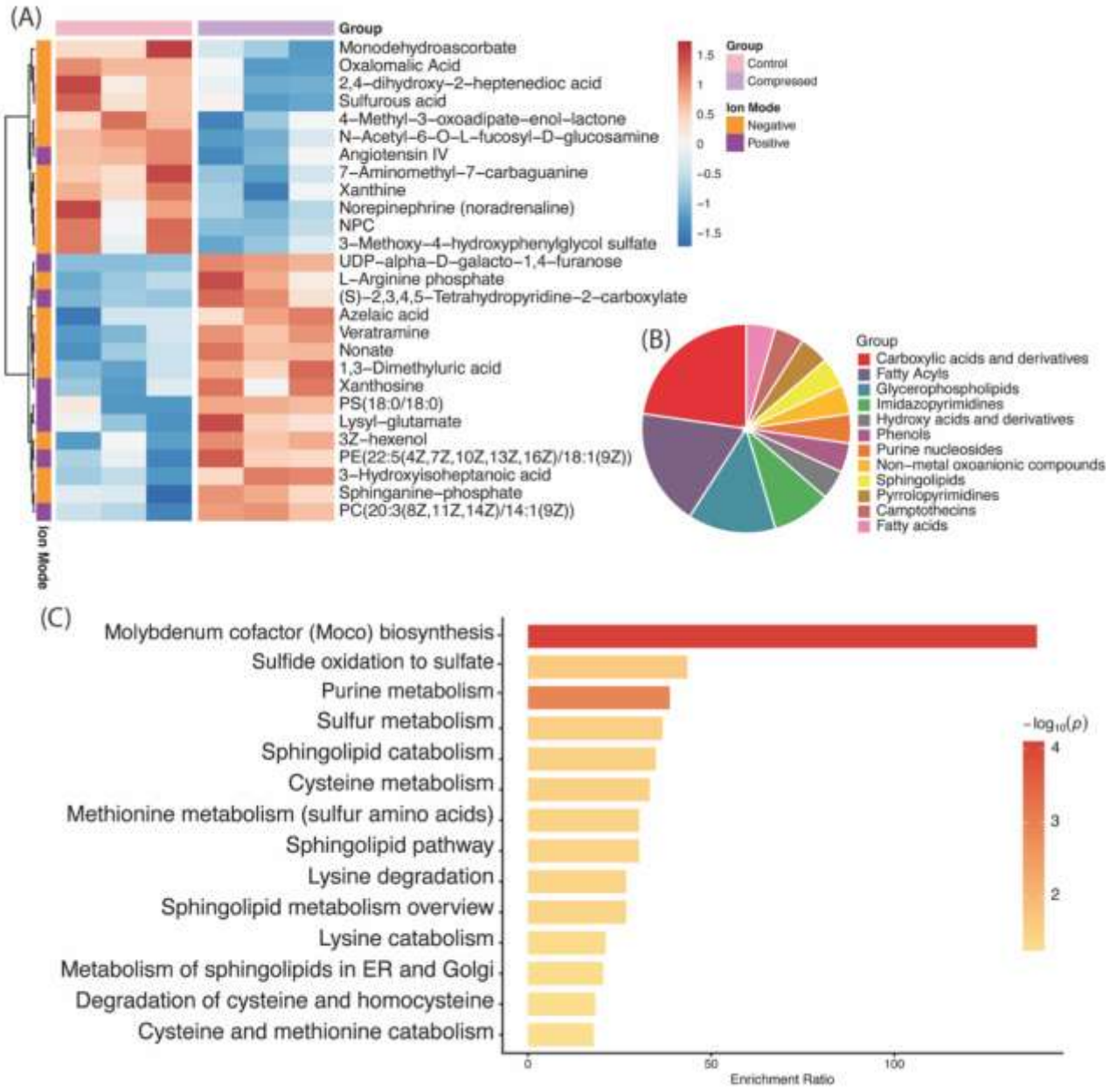



**Figure 6.Exometabolomic profiling reveals structured metabolic remodeling under mechanical compression in MIA PaCa-2 cells.** (A) Heatmap of 27 significantly altered metabolites ($p < 0.05$ and $|log2FC| >= 1.0$) in conditioned media from compressed versus control MIA PaCa-2 cells. Metabolites were detected across negative and positive electrospray ionization modes (annotated as Ion Mode). Intensities were log10-transformed, Pareto-scaled across all samples (including cell-free media), and Z-score normalized per metabolite for visualization. Hierarchical clustering used Euclidean distance with Ward's D2 linkage. Columns are ordered by group (control, then compressed) with a gap separating conditions. (B) Compound class distribution of significantly altered metabolites annotated using MetaboAnalyst's chemical taxonomy. (C) Metabolite set enrichment analysis (MSEA) of significantly altered metabolites using over-representation analysis (ORA) against the RaMP pathway library. Bar length represents enrichment ratio; color intensity indicates statistical significance (-log10 p-value). Pathways were curated to retain 14 biologically meaningful categories across four functional themes: purine metabolism, sulfur/redox metabolism, sphingolipid signaling, and amino acid catabolism. Rare inherited disease annotations, drug metabolism pathways, and neuropsychiatric terms were excluded. All statistical tests were performed via the MetaboAnalyst 6.0 web platform.

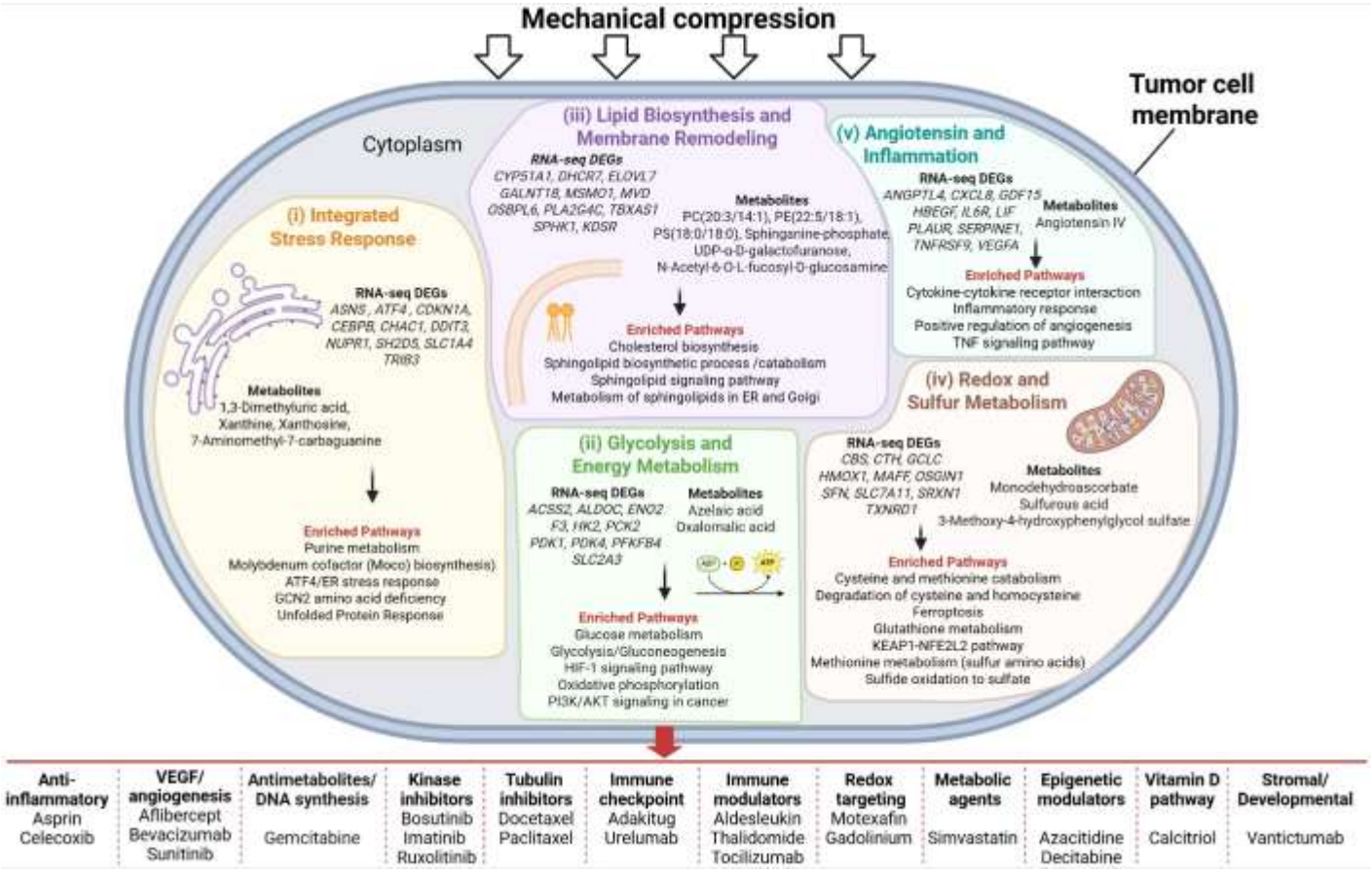



**Figure 7. Multi-omics pathway convergence under mechanical compression in MIA PaCa-2 pancreatic cancer cells.** Schematic representation of pathway-level convergence across RNA-seq transcriptomics, LC-MS exometabolomics, and drug-gene interaction analysis in MIA PaCa-2 cells subjected to 4 mmHg compressive stress for 24 h. The central cell schematic depicts five convergence hubs mapped to subcellular compartments where transcriptomic, metabolomic, and pathway enrichment evidence intersect: (i) The Integrated Stress Response hub (endoplasmic reticulum) (ii) The Glycolysis and Energy Metabolism hub (cytoplasm) (iii) The Lipid Biosynthesis and Membrane Remodeling hub (plasma membrane/Golgi) (iv) The Redox and Sulfur Metabolism hub (mitochondria/cytoplasm) and (v) The Angiogenesis and Inflammation hub (secreted/extracellular). The bottom layer displays 23 PDAC-investigated drugs organized by mechanism of action (COX/anti-inflammatory, antimetabolites/DNA synthesis, VEGF/angiogenesis, kinase inhibitors, tubulin inhibitors, immunomodulatory, immune checkpoint, epigenetic modulators, metabolic agents, redox targeting, vitamin D pathway, stroma/developmental), derived from DGIdb 5.0 (interaction score ≥ 0.1) cross-validated against the Open Targets Platform using verified PDAC disease identifiers. Drug–gene connections span all five hubs, with Hub (v) representing the most pharmacologically dense node. Convergence hubs represent pathway-level concordance across omics layers and do not imply formal multi-omics factor analysis, which is not appropriate for the current sample size (n = 3 per condition). Created with BioRender.com.

## Discussion

Our study demonstrates that mechanical compression induces extensive and tumor type-dependent transcriptional and metabolic reprogramming and that compression-associated gene expression programs are detectable in patient tumors, associate with clinical outcome, and intersect with therapeutic targets currently investigated in solid malignancies. Together, our findings position tumor compression as a biologically and clinically relevant variable that operates independently of tumor-intrinsic genomic alterations and suggest that the physical microenvironment constitutes an underappreciated axis influencing therapeutic response that is not captured by current precision oncology frameworks.

Our transcriptomic analyses show that mechanical compression activates stress-adaptive pathways with known links to treatment response. In pancreatic cancer cells, compression induced a transcriptional state dominated by the integrated stress response (ISR) (33-36), including PERK-regulated gene expression, EIF2AK4/GCN2 signaling, and ATF4-dependent targets. The ISR is a conserved cytoprotective program that rewires translation and metabolism in response to cellular stress and has been implicated in chemotherapy resistance in pancreatic cancer. Prior studies have shown that inhibition of ISR signaling, including ATF4 depletion or pharmacological ISR blockade, enhances gemcitabine-induced apoptosis, supporting a role for this pathway in therapy tolerance. Our finding that mechanical compression activates this program suggests that mechanical forces within the tumor microenvironment may contribute to reduced chemotherapy sensitivity through mechanisms that are independent of acquired genetic alterations (35, 37).

Compression also activated the KEAP1–NRF2 antioxidant axis, including canonical NRF2-responsive genes. NRF2-dependent programs regulate redox homeostasis and detoxification and have been associated with resistance to multiple anticancer agents, including gemcitabine, cisplatin, and 5-fluorouracil. In pancreatic cancer models, NRF2 depletion has been reported to increase drug sensitivity and suppress proliferation. The concurrent activation of ISR and NRF2 pathways observed here therefore suggests that compression may establish a coordinated cytoprotective state capable of buffering therapeutic stress in compressed tumor regions (38-40).

At the same time, compression strongly suppressed cell-cycle and mitotic programs, including genes involved in DNA replication, chromosome segregation, and S-phase progression. This observation may have therapeutic implications, as several frontline anticancer agents rely on active cancer cell proliferation for their cytotoxic efficacy, antimetabolites such as gemcitabine and 5-fluorouracil exert their effects by disrupting DNA synthesis during S-phase, while microtubule-targeting drugs interfere with mitotic spindle assembly during cell division (41-43). Compression-induced suppression of proliferative gene programs in cancer cells may therefore reduce their susceptibility to these agents by limiting the cellular processes these drugs target, although direct functional validation will be required to confirm this interpretation.

The metabolomic analysis of pancreatic cancer cells provides orthogonal support for these transcriptional findings and further suggests the emergence of a coordinated compression-induced metabolic state. Compression altered extracellular metabolite profiles linked to purine metabolism, sphingolipid remodeling, and sulfur-dependent redox pathways. These changes aligned closely with the transcriptional programs identified by RNA-seq: altered purine-related metabolites were consistent with ISR-associated metabolic adaptation, sphingolipid remodeling paralleled coordinated transcriptional changes in SPHK1, KDSR, and CERS1, and

sulfur pathway enrichment converged with activation of the KEAP1-NFE2L2 antioxidant axis. Notably, the most significantly enriched pathway was molybdenum cofactor biosynthesis, which generates a sulfur-containing cofactor required for redox enzymes involved in oxidative metabolism and xenobiotic detoxification (44-46), further linking compression-induced metabolic adaptation to pathways relevant for drug handling.

Our drug–gene interaction analysis further showed that compression-responsive genes intersect with several therapeutic targets currently being explored in pancreatic cancer. Genes upregulated under compression included direct or inferred targets of agents under clinical investigation, such as VEGFA, CXCL8, IL6R, and TNFRSF9. These observations indicate that compression can reshape the expression of molecules that are themselves pharmacologically actionable. More broadly, they suggest that mechanical stress may influence treatment response not simply by altering upstream signaling, but by modifying the transcriptional and metabolic context in which drug targets function. Importantly, however, the directionality of this effect remains unresolved. Compression-induced reprogramming may either create context-specific therapeutic vulnerabilities by increasing dependence on certain pathways, or alternatively promote adaptive states that reduce drug sensitivity, for example through stress-response activation or proliferative suppression.

Importantly, compression-induced programs differed substantially across tumor types. In breast cancer cells, compression preferentially activated immediate-early stress response regulators and plasticity-associated transcription factors, including JUN, MYC, CEBPB, ATF3, and SNAI1. Prior work has linked ATF3 to multidrug resistance (47) and SNAI1 to epithelial–mesenchymal transition, invasiveness, stem-like behavior, and resistance to systemic therapy (48, 49), raising the possibility that mechanical stress may promote a therapy-tolerant and plastic cellular state in this context. In hepatocellular carcinoma cells, by contrast, compression induced programs dominated by extracellular matrix organization and angiogenic signaling, including VEGFA, PDGFB, ANGPTL4, and AXL. This pattern is consistent with the fibrotic and mechanically abnormal liver tumor microenvironment and with prior studies implicating mechanotransduction pathways in liver cancer progression and vascular remodeling angiogenesis (50). Together, these observations suggest that compression engages a broadly conserved stress-adaptation framework that is integrated into lineage-specific regulatory circuitry.

Across all three tumor types, compression-responsive transcriptional programs were largely independent of the intrinsic genomic landscape. DepMap analyses showed that the vast majority of compression-regulated genes were genomically unaltered, including key mechanosensitive regulators such as FOS, JUN, VEGFA, ANGPTL4, and GADD45A. Moreover, mutation-enriched pathways were distinct from compression-induced pathways, indicating that mechanical stress represents an additional layer of tumor cell plasticity rather than a direct consequence of pre-existing genomic alterations. This dissociation between genotype and mechanically induced phenotype has important implications for precision oncology, as transcriptional states relevant to drug response may arise from physical microenvironmental conditions that are not captured by genomic profiling alone.

Finally, analysis of patient transcriptomes suggests that compression-associated transcriptional states may have clinical relevance. Compression signatures derived from our in vitro datasets were detectable in patient tumors and were associated with worse unadjusted survival in pancreatic and liver cancer cohorts. However, the effect was attenuated after

multivariable adjustment, and confidence intervals were wide, particularly in pancreatic cancer, indicating that the prognostic contribution of these signatures should be interpreted cautiously and validated in larger, independent cohorts. Even so, the presence of these programs in patient tumors supports the translational relevance of the compression-associated states identified experimentally.

Taken together, our findings support a model in which tumor compression establishes a distinct mechanoadaptive cellular state characterized by coordinated transcriptional and metabolic remodeling that intersects with multiple therapeutic pathways. Precision oncology approaches based solely on tumor-intrinsic molecular alterations may therefore overlook an important dimension of tumor biology. Incorporating mechanical microenvironmental features and compression-associated molecular signatures into biomarker frameworks may improve the prediction of therapeutic response in mechanically aberrant solid tumors.

## Limitations and conclusion

Our analyses were performed in cell line models under static compression conditions, which do not fully recapitulate the dynamic and spatially heterogeneous nature of mechanical stress in vivo. Exometabolomic profiling captured extracellular metabolic flux as a proxy for intracellular metabolic state, and the modest sample size limits pathway-level statistical power. Compression signatures were derived from in vitro data and applied to patient transcriptomes without direct measurement of intratumoral forces, which remains technically challenging in clinical settings. Functional validation of compression-induced resistance mechanisms through pharmacological perturbation and in vivo models will be an important next step. Despite the limitations, our study provides a first systematic integration of tumor compression into a multi-omics precision oncology framework. The convergence of transcriptomic, metabolomic, pharmacogenomic, and clinical evidence supports the conclusion that mechanical compression establishes a coordinated cellular state that intersects with major therapeutic axes in solid tumors. Precision oncology strategies based exclusively on tumor-intrinsic molecular features are incomplete if they do not account for how the physical microenvironment reshapes the transcriptional and metabolic landscape that drugs encounter. Incorporating compression-associated molecular signatures into patient stratification frameworks represents a promising and underexplored direction for improving therapeutic outcomes in mechanically aberrant solid tumors.

## Acknowledgements

This project received funding from the European Research Council (ERC) under the European Union's Horizon Europe research and innovation programme (Grant Agreement No. 101141357), awarded to T.S. Views and opinions expressed are however those of the authors only and do not necessarily reflect those of the European Union or the European Research Council Executive Agency. Neither the European Union nor the granting authority can be held responsible for them.

## Declarations

The authors declare that they have no competing interests.

## Author contributions

S. G. performed the bioinformatics analyses and wrote the manuscript; C.S. performed *in vitro* experiments; S.K., E.H., and F.M. performed LC-MS–based exometabolomics analyses; C.V. supervised bioinformatics analyses and edited the manuscript; T.S. conceived study, supervised research, acquired funding and edited the manuscript; M.K. conceived and designed the study, supervised research and wrote the manuscript; All authors reviewed, revised, and approved the final manuscript.

**References**


1. Hanahan D, Weinberg RA. Hallmarks of cancer: the next generation. Cell. 2011;144(5):646-74.
2. Holohan C, Van Schaeybroeck S, Longley DB, Johnston PG. Cancer drug resistance: an evolving paradigm. Nat Rev Cancer. 2013;13(10):714-26.
3. Marine JC, Dawson SJ, Dawson MA. Non-genetic mechanisms of therapeutic resistance in cancer. Nat Rev Cancer. 2020;20(12):743-56.
4. Ghorbian S. Cancer cell plasticity and therapeutic resistance: mechanisms, crosstalk, and translational perspectives. Hereditas. 2025;162(1):188.
5. Chang K, Creighton CJ, Davis C, Donehower L, Drummond J, Wheeler D, et al. The Cancer Genome Atlas Pan-Cancer analysis project. Nature Genetics. 2013;45(10):1113-20.
6. Hudson TJ, Anderson W, Artez A, Barker AD, Bell C, Bernabé RR, et al. International network of cancer genome projects. Nature. 2010;464(7291):993-8.
7. Akhoundova D, Rubin MA. Clinical application of advanced multi-omics tumor profiling: Shaping precision oncology of the future. Cancer Cell. 2022;40(9):920-38.
8. Sicklick JK, Kato S, Okamura R, Schwaederle M, Hahn ME, Williams CB, et al. Molecular profiling of cancer patients enables personalized combination therapy: the I-PREDICT study. Nat Med. 2019;25(5):744-50.
9. Chakravarty D, Solit DB. Clinical cancer genomic profiling. Nat Rev Genet. 2021;22(8):483-501.
10. Quail DF, Joyce JA. Microenvironmental regulation of tumor progression and metastasis. Nat Med. 2013;19(11):1423-37.
11. Stylianopoulos T, Martin JD, Chauhan VP, Jain SR, Diop-Frimpong B, Bardeesy N, et al. Causes, consequences, and remedies for growth-induced solid stress in murine and human tumors. Proc Natl Acad Sci U S A. 2012;109(38):15101-8.
12. Stylianopoulos T, Martin JD, Snuderl M, Mpekris F, Jain SR, Jain RK. Coevolution of solid stress and interstitial fluid pressure in tumors during progression: implications for vascular collapse. Cancer Res. 2013;73(13):3833-41.
13. Jain RK, Martin JD, Stylianopoulos T. The role of mechanical forces in tumor growth and therapy. Annu Rev Biomed Eng. 2014;16:321-46.
14. Chauhan VP, Stylianopoulos T, Martin JD, Popović Z, Chen O, Kamoun WS, et al. Normalization of tumour blood vessels improves the delivery of nanomedicines in a size-dependent manner. Nat Nanotechnol. 2012;7(6):383-8.
15. Mpekris F, Angeli S, Pirentis AP, Stylianopoulos T. Stress-mediated progression of solid tumors: effect of mechanical stress on tissue oxygenation, cancer cell proliferation, and drug delivery. Biomech Model Mechanobiol. 2015;14(6):1391-402.
16. Kalli M, Poskus MD, Stylianopoulos T, Zervantonakis IK. Beyond matrix stiffness: targeting force-induced cancer drug resistance. Trends Cancer. 2023;9(11):937-54.
17. Zhang M, Zhang B. Extracellular matrix stiffness: mechanisms in tumor progression and therapeutic potential in cancer. Exp Hematol Oncol. 2025;14(1):54.
18. Sievers J, Mahajan V, Welzel PB, Werner C, Taubenberger A. Precision Hydrogels for the Study of Cancer Cell Mechanobiology. Adv Healthc Mater. 2023;12(14):e2202514.
19. Aydin HB, Ozcelikkale A, Acar A. Exploiting Matrix Stiffness to Overcome Drug Resistance. ACS Biomater Sci Eng. 2024;10(8):4682-700.

20. LeSavage BL, Zhang D, Huerta-López C, Gilchrist AE, Krajina BA, Karlsson K, et al. Engineered matrices reveal stiffness-mediated chemoresistance in patient-derived pancreatic cancer organoids. Nature Materials. 2024;23(8):1138-49.
21. Chen Y, Xue D, Huang D, Li X, Duan Y, Chen B. Biofabrication of Tunable 3D Hydrogel for Investigating the Matrix Stiffness Impact on Breast Cancer Chemotherapy Resistance. ACS Biomaterials Science & Engineering. 2025;11(3):1417-31.
22. Nia HT, Liu H, Seano G, Datta M, Jones D, Rahbari N, et al. Solid stress and elastic energy as measures of tumour mechanopathology. Nat Biomed Eng. 2016;1.
23. Kalli M, Stylianopoulos T. Defining the Role of Solid Stress and Matrix Stiffness in Cancer Cell Proliferation and Metastasis. Front Oncol. 2018;8:55.
24. Kalli M, Li R, Mills GB, Stylianopoulos T, Zervantonakis IK. Mechanical Stress Signaling in Pancreatic Cancer Cells Triggers p38 MAPK- and JNK-Dependent Cytoskeleton Remodeling and Promotes Cell Migration via Rac1/cdc42/Myosin II. Mol Cancer Res. 2022;20(3):485-97.
25. Kalli M, Minia A, Pliaka V, Fotis C, Alexopoulos LG, Stylianopoulos T. Solid stress-induced migration is mediated by GDF15 through Akt pathway activation in pancreatic cancer cells. Scientific Reports. 2019;9(1):978.
26. Kalli M, Papageorgis P, Gkretsi V, Stylianopoulos T. Solid Stress Facilitates Fibroblasts Activation to Promote Pancreatic Cancer Cell Migration. Ann Biomed Eng. 2018;46(5):657-69.
27. Kalli M, Voutouri C, Minia A, Pliaka V, Fotis C, Alexopoulos LG, et al. Mechanical Compression Regulates Brain Cancer Cell Migration Through MEK1/Erk1 Pathway Activation and GDF15 Expression. Front Oncol. 2019;9:992.
28. Kalli M, Mpekris F, Charalambous A, Michael C, Stylianou C, Voutouri C, et al. Mechanical forces inducing oxaliplatin resistance in pancreatic cancer can be targeted by autophagy inhibition. Communications Biology. 2024;7(1):1581.
29. Azizan F, Sheriff RS, Goh CJH, Chiam KH, Koh CG. Solid stress compression enhances breast cancer cell migration through the upregulation of Interleukin-6. Front Cell Dev Biol. 2025;13:1541953.
30. Gong X, Ogino N, Leite MF, Zhang D, Chen Z, Nguyen RY, et al. Adaptation to Volumetric Compression Drives an Apoptosis-Resistant and Invasive Phenotype in Liver Cancer. Cancer Res. 2025;85(16):3156-75.
31. Barbie DA, Tamayo P, Boehm JS, Kim SY, Moody SE, Dunn IF, et al. Systematic RNA interference reveals that oncogenic KRAS-driven cancers require TBK1. Nature. 2009;462(7269):108-12.
32. Cannon M, Stevenson J, Stahl K, Basu R, Coffman A, Kiwala S, et al. DGIdb 5.0: rebuilding the drug-gene interaction database for precision medicine and drug discovery platforms. Nucleic Acids Res. 2024;52(D1):D1227-d35.
33. Lines CL, McGrath MJ, Dorwart T, Conn CS. The integrated stress response in cancer progression: a force for plasticity and resistance. Front Oncol. 2023;13:1206561.
34. Costa-Mattioli M, Walter P. The integrated stress response: From mechanism to disease. Science. 2020;368(6489).
35. Pakos-Zebrucka K, Koryga I, Mnich K, Ljujic M, Samali A, Gorman AM. The integrated stress response. EMBO Rep. 2016;17(10):1374-95.
36. Malnassy G, Ziolkowski L, Macleod KF, Oakes SA. The Integrated Stress Response in Pancreatic Development, Tissue Homeostasis, and Cancer. Gastroenterology. 2024;167(7):1292-306.

37. Koltai T, Reshkin SJ, Carvalho TMA, Di Molfetta D, Greco MR, Alfarouk KO, et al. Resistance to Gemcitabine in Pancreatic Ductal Adenocarcinoma: A Physiopathologic and Pharmacologic Review. Cancers (Basel). 2022;14(10).
38. Bae ES, Byun WS, Ock CW, Kim WK, Park HJ, Lee SK. Periplocin exerts antitumor activity by regulating Nrf2-mediated signaling pathway in gemcitabine-resistant pancreatic cancer cells. Biomed Pharmacother. 2023;157:114039.
39. Solis LM, Behrens C, Dong W, Suraokar M, Ozburn NC, Moran CA, et al. Nrf2 and Keap1 abnormalities in non-small cell lung carcinoma and association with clinicopathologic features. Clin Cancer Res. 2010;16(14):3743-53.
40. Matsumoto R, Hamada S, Tanaka Y, Taguchi K, Yamamoto M, Masamune A. Nuclear Factor Erythroid 2-Related Factor 2 Depletion Sensitizes Pancreatic Cancer Cells to Gemcitabine via Aldehyde Dehydrogenase 3a1 Repression. J Pharmacol Exp Ther. 2021;379(1):33-40.
41. Jia Y, Xie J. Promising molecular mechanisms responsible for gemcitabine resistance in cancer. Genes Dis. 2015;2(4):299-306.
42. Zhang N, Yin Y, Xu SJ, Chen WS. 5-Fluorouracil: mechanisms of resistance and reversal strategies. Molecules. 2008;13(8):1551-69.
43. Serpico AF, Visconti R, Grieco D. Exploiting immune-dependent effects of microtubule-targeting agents to improve efficacy and tolerability of cancer treatment. Cell Death Dis. 2020;11(5):361.
44. Schwarz G. Molybdenum cofactor biosynthesis and deficiency. Cell Mol Life Sci. 2005;62(23):2792-810.
45. Adamus JP, Ruszczyńska A, Wyczałkowska-Tomasik A. Molybdenum's Role as an Essential Element in Enzymes Catabolizing Redox Reactions: A Review. Biomolecules. 2024;14(7).
46. Michael M, Doherty MM. Tumoral drug metabolism: overview and its implications for cancer therapy. J Clin Oncol. 2005;23(1):205-29.
47. Chang YS, Jalgaonkar SP, Middleton JD, Hai T. Stress-inducible gene Atf3 in the noncancer host cells contributes to chemotherapy-exacerbated breast cancer metastasis. Proc Natl Acad Sci U S A. 2017;114(34):E7159-e68.
48. Lim S, Becker A, Zimmer A, Lu J, Buettner R, Kirfel J. SNAI1-mediated epithelial-mesenchymal transition confers chemoresistance and cellular plasticity by regulating genes involved in cell death and stem cell maintenance. PLoS One. 2013;8(6):e66558.
49. Pinto E, Pelizzaro F, Farinati F, Russo FP. Angiogenesis and Hepatocellular Carcinoma: From Molecular Mechanisms to Systemic Therapies. Medicina (Kaunas). 2023;59(6).
50. Li N, Zhang X, Zhou J, Li W, Shu X, Wu Y, et al. Multiscale biomechanics and mechanotransduction from liver fibrosis to cancer. Adv Drug Deliv Rev. 2022;188:114448.